INVERTED MICELLAR STRUCTURES IN BILAYER MEMBRANES

Formation Rates and Half-Lives

D. P. SIEGEL
The Procter and Gamble Company, Miami Valley Laboratories, Cincinnati, Ohio 45247

ABSTRACT Two sorts of inverted micellar structures have previously been proposed to explain morphological and ^{31}P-NMR observations of bilayer systems. These structures only form in systems with components that can adopt the inverse hexagonal (H_{II}) phase. LIP (lipidic particles) are intrabilayer structures, whereas IMI (inverted micellar intermediates) are structures that form between apposed bilayers. Here, we calculate the formation rates and half-lives of these structures to determine which (or if either) of these proposed structures is a likely explanation of the data. Calculations for the egg phosphatidylethanolamine and the Ca^{+}-cardiolipin systems show that IMI form orders of magnitude faster than LIP, which should form slowly, if at all. This result is probably true in general, and indicates that "lipidic particle" electron micrograph images probably represent interbilayer structures, as some have previously proposed. It is shown here that IMI are likely intermediates in the lamellar $\leftrightarrow$ H_{II} phase transitions and in the process of membrane fusion in some systems. The calculated formation rates, half-lives, and vesicle-vesicle fusion rates are in agreement with this observation.

INTRODUCTION

Many authors have invoked inverted micellar structures to explain the morphology and ^{31}P-NMR spectra associated with nonbilayer structures in lipid systems near the lamellar-to-inverted hexagonal (H_{II}) phase transition (1–10). Freeze-fracture electron micrographs of multilamellar preparations show corresponding bulges and pits in the lipid lamellae, ~10 nm in diameter. These have been called "lipidic particles" (LIP) (e.g., 1, 6). Inverted micelles are good candidates for the components of such structures. They have appropriate radii of curvature and resemble the H_{II} phase (water enveloped by lipid). Presumably, on account of this resemblance, inverted micellar structures can form most rapidly near the spontaneous lamellar-to-H_{II} transition. These are, in fact, the conditions under which LIP are observed. The ^{31}P-NMR spectra of some phospholipid systems near the lamellar-to-H_{II} phase transition contain "isotropic" components: These are thought to be due to the motion of lipids around radii of curvature similar to those expected in inverted micellar structures (6, 10). However, such resonances might be due to a variety of structures with small radii, such as cubic phases or even small vesicles (e.g., 11).

Two types of inverted micellar structural models for lipidic particles have been proposed. The first is referred to here as the LIP because it was the first inverted micellar model associated with the observations (1, 6). LIP are intrabilayer structures, assumed (1–8) to be spherical inverted micelles sandwiched between the monolayers of the bilayer (see Fig. 1). The second is the IMI (inverted micellar intermediate), a spherical inverted micelle within a cusplike interbilayer attachment (Fig. 2). This sort of structure has been proposed (e.g., 2, 5, 12–14, 15) as a transient intermediate in the process of membrane fusion and the lamellar-to-H_{II} phase transition.

There is debate as to which (or if either) of these structures best describes the morphological and NMR data (e.g., 3, 12, 16, 17). LIP and IMI are potentially important in the dynamics of pure lipid systems and biomembranes (2, 5, 12–15, 18); they could be involved in membrane fusion, interbilayer and transbilayer movement of lipids and other substances. When we have a better understanding of lipidic particle sturcture, formation rates, and half-lives, we will be able to make more quantitative estimates of the effects of these structures on biomembrane properties.

In this paper, I have derived expressions for the formation rates and half-lives of these two hypothetical inverted micellar structures. The general approach is as follows. LIP or IMI formation is viewed as a two-step process. First, enough lipid molecules must be assembled (by concentration fluctuations in the plane of the bilayer) in one spot to form a LIP or IMI. The required number and area can be calculated using the dimensions of the bilayer and H_{II} phases. The probability of a critical fluctuation can be calculated using simple thermodynamics and the bilayer lateral compressibility (obtainable via two different

methods). Second, one calculates the probability of LIP formation from patches of interface undergoing a critical fluctuation. This probability is expressed as the product of an Arrhenius rate constant and the lifetime of the fluctuation. The lifetime is the random-walk diffusion time of a lipid molecule across the area of interface involved. The frequency factor and activation energy of the rate constant can be estimated using the time scales of lipid motion in the bilayer phase and the thermodynamics of the lamellar-to-H_{II} transition, respectively. In the case of the IMI, the probability that the interfaces of the two bilayers are closely apposed during the critical fluctuation must also be considered. Close apposition must occur so that the motions of lipids in both interfaces can become cooperative. Close apposition is taken to mean interfacial separations of <1 nm.

Expressions describing LIP formation are derived in the first part of section A entitled One-Component Systems. The second and third parts entitled Formation of LIP in Two-Component Systems and Conclusions Concerning the LIP Model contain a derivation of the effects of impurities on formation rates and a discussion of results, respectively. IMI formation rates are derived in section B, in the first part entitled Theory, and are discussed in the final part entitled Conclusions Concerning IMI. Readers who are more interested in the physical significance of the results than the details of the derivations need read only the last part of sections A and B.

The results can be briefly summarized. LIP, the intrabilayer structures, are predicted to form extremely slowly. Sample calculations for egg phosphatidylethanolamine (EPE) and the Ca^{+2}-cardiolipin (Ca^{+2}-CL) systems show that LIP would form at a maximum rate of hundreds of structures per square micron of bilayer per hour; this is, if anything, an over-estimate. This is consistent with the absence of LIP in unilamellar phosphatidylethanolamine (PE) dispersions (17), and the very slow appearance of such structures in unilamellar cardiolipin-phosphatidylcholine preparations exposed to Ca^{+2} (19). LIP are predicted to have very long half-lives, though they are not thermodynamically stable structures.

However, IMI (the interbilayer structures) should form quite rapidly. It will be shown that the formation of such structures requires either no fluctuation or very small fluctuations in the local lipid concentration in the bilayers. Moreover, the activation energy for inverted micelle formation is likely to be much smaller then for LIP. This accounts for the high frequency of lipidic particle images in multi- (as opposed to uni-) lamellar dispersions. IMI can only form between two or more membranes, a situation ubiquitous in liposomes but rarer in dispersions of unilamellar vesicles. In some cases the rate-limiting step in IMI formation is the rate at which membranes can be closely apposed. Under the right conditions, IMI will form between closely apposed EPE and Ca^{+2}-CL interfaces in milliseconds or less.

IMI may be intermediates in the process of membrane fusion. Our work predicts that IMI can spontaneously revert to bilayer structure (Fig. 2), either fusing the two apposed bilayers (bottom left of Fig. 2) or reforming the original bilayers (bottom right). Fusion in this fashion results in cusplike interbilayer attachments such as those observed by others (12, 16, 17).

IMI could also be intermediates in the $L \rightarrow H_{II}$ phase transition. Above the bulk $L \rightarrow H_{II}$ phase transition of the apposed bilayers, the rate of IMI reversion is slow, and IMI should exist long enough to aggregate with others into H_{II} rod precursors (Fig. 4). Various workers have commented on the tendency of lipidic particle-like structures to form linear arrays (e.g., 3, 6, 16) and appear to form or bleb off from H_{II}-like tubes (e.g., 5, 8, 20). In some systems (2, 20) there is evidence for a cubic phase consisting of arrays of inverted micelles, which could form via an analogous mechanism. However, the exact nature of these structures is uncertain (21).

The half-lives of IMI for EPE and Ca^{+2}-CL are predicted in the 0.1-ms range under most circumstances. This makes imaging of IMI via electron microscopy very difficult, even using rapid-freezing techniques. These short half-lives may also explain the absence or near absence of isotropic ^{31}P-NMR resonances from pure unsaturated alkyl chain-PE preparations (22, 23) and Ca^{+2}-CL systems (24) under conditions when IMI reversion is rapid. Such resonances are observed under conditions for which we predict longer IMI half-lives (24–26). The model of IMI as intermediates in the $L \leftrightarrow H_{II}$ phase transitions is also compatible with the temperature and Ca^{+2} concentration hysteresis observed in the EPE (23, 27) and Ca^{+2}-CL (24, 28) systems.

We also calculate rate constants for the fusion of pairs of aggregated unilamellar vesicles via IMI. The results seem compatible with observations on related lipid systems. Fusion via IMI is predicted to occur at slow rates in EPE systems and quite rapidly in Ca^{+2}-CL systems. These rates are, respectively, slower than and faster than the rate of vesicle fusion in the Ca^{+2}-PS system (29–35), which clearly proceeds via a different mechanism. Since at least one other fusion mechanism exists, it may be difficult to determine the relative contribution (if any) of IMI fusion to the observed rate in H_{II} phase-forming systems. Our work identifies some criteria for making this distinction. However, IMI-mediated fusion remains to be unequivocally demonstrated.

A. FORMATION OF INVERTED MICELLAR STRUCTURES (LIP) IN ISOLATED BILAYERS

One-Component Systems

First, we must determine the number of molecules necessary to form an LIP structure. We start with the assumption that the area per lipid molecule, a_o, at the lipid-water

interface within the inverted micelle is the same as at the interface in the H_{II} phase. Moreover, we assume that the radius, r_i, of the water cavity within the inverted micelle (see Fig. 1) is at least as large as the radius of the water channel in the H_{II} phase, r_H. This is reasonable, because the cavity in the inverted micelle has two small principal radii of curvature, whereas the water channel in the H_{II} phase has only one. We would expect that, if anything, lipid-packing constraints in the micelle would be more severe than in the H_{II} phase, making $r_i > r_H$. The number of molecules, n_m, composing the micelle is then simply the surface area of the water cavity divided by a_o,

$$n_m = \frac{4\pi r_i^2}{a_o}. \tag{1}$$

The radius of the entire micelle is the water cavity radius plus the thickness of a lipid monolayer, ℓ

$$r_m = r_i + \ell. \tag{2}$$

We must also calculate the number of lipid molecules in the curved monolayers enveloping the inverted micelle. The structure of these monolayers is significantly different from bilayer structure for a radius equal to $r_m + \ell$ around the center of the micelle (Fig. 1). Therefore, all molecules of the exterior monolayers within this distance from the center of the micelle are assumed part of the LIP. Simple geometric arguments show that the number of lipid molecules in each exterior monolayer (n_e) is

$$n_e \simeq \frac{2\pi}{\bar{a}}\left[(r_m + \ell/2)^2 - \frac{\ell(r_m + \ell/2)^2}{(r_m + \ell)} + \frac{\ell^2}{2}\right], \tag{3}$$

where $\bar{a}$ is the equilibrium area per lipid molecule at the bilayer/water interface. To evaluate n_e, we have calculated the surface area of each enveloping monolayer at the monolayer midplane (i.e., at a radius of $r_m + \ell/2$ from the center of the micelle) and divided by $\bar{a}$. This is appropriate because of the small radii of curvature of these surfaces. The number of lipid molecules composing the LIP is $n_m + 2n_e$. The number of molecules normally occupying a circular patch of bilayer/water interface of radius $r_m + \ell$ at equilibrium coverage is simply

$$\bar{n} = \frac{\pi(r_m + \ell)^2}{\bar{a}}. \tag{4}$$

Given the number of molecules comprising an LIP ($2n_e + n_m$) and the number of molecules normally found in a patch of bilayer of the same cross-sectional area ($A = \pi[r_m + \ell]^2$), we can calculate the probability that lipid concentration fluctuations in the two leaflets of the bilayer will assemble the requisite number of molecules in the same spot. Fluctuations in the two monolayer leaflets of the bilayer are assumed independent. This assumption is reasonable: the coupling between the leaflets during phase transitions is very weak (36–38); defects due to population dissymmetry in the leaflets of unilamellar vesicles heal quite slowly (39); and the order parameter of the terminal methyl and methylene groups of the phospholipid alkyl chains is quite low, so we would expect changes in packing within one monolayer to only weakly influence packing in the other. This weak coupling assumption may break down for dialkyl glycerolipids with alkyl chains of greatly different length (differences > two methylene groups, [37]).

The difference between one-half the number of molecules necessary to form a LIP and $\bar{n}$ is Δn,

$$\Delta n = \frac{1}{2}(n_m + 2n_e) - \bar{n}. \tag{5}$$

The relative magnitude of the critical fluctuation, $\tilde{n}_c$ (which is the fluctuation large enough to permit LIP formation) is then

$$\tilde{n}_c = \frac{\Delta n}{\bar{n}} = \frac{(n_m + 2n_e)}{2\bar{n}} - 1. \tag{6}$$

(Naturally, the values of n_m, n_e, and $\bar{n}$ in this expression should be integers.) The probability of a fluctuation of this magnitude in each monolayer is calculated in the fashion of Blank (40). The fluctuation amplitudes in a monolayer patch of area A at temperature T are assumed to be Gaussian distributed. The root mean squared (rms) amplitude is given by

$$\left(\frac{\Delta n}{\bar{n}}\right) = \frac{kTC_s}{A}, \tag{7}$$

where

$$C_s = -\frac{1}{A}\left(\frac{\partial A}{\partial \Pi}\right)_T. \tag{8}$$

C_s is the lateral compressibility of the lipid monolayer and Π is the lateral pressure in the plane of the monolayer. k is Boltzmann's constant.

Values of C_s can be obtained from Langmuir trough measurements (preferably at the oil-water interface), or from x-ray studies of bilayer systems via the method of Lis

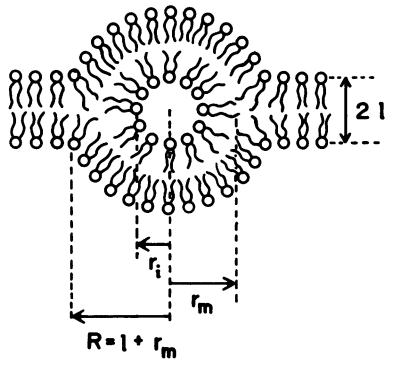

FIGURE 1 LIP structure in cross section. The inverted micelle is spherical. The structure is cylindrically symmetrical about the vertical axis (dashed line through the center of the micelle).

et al. (41). In principle, C_s of monolayers at the oil-water interface should approximate the bilayer compressibility. This is more obvious if, instead of $(\partial A/\partial \Pi)$, we consider the change of volume of each system at constant monolayer thickness, h, compressed by an amount $\Delta\alpha$. That is,

$$\left(\frac{\partial A}{\partial \Pi}\right)_T \approx \frac{1}{h}\left(\frac{\Delta \text{ volume}}{\Delta \Pi}\right)_{\text{constant } h}. \quad (9)$$

If a force, F, is required to produce a small compression, $\Delta\alpha$, in a bilayer, the derivative in Eq. 9 is $\sim 2\Delta\alpha h/F$. If the monolayers behave independently, a monolayer can be compressed to the same $\Delta\alpha$ by $F/2$, with a volume change of only $\Delta\alpha h$. The compressibility is thus the same as in the bilayer case. The assumption of constant monolayer thickness is valid for small fluctuations in lipid concentration.

The standard deviation of the distribution of n is then

$$\sigma = \bar{n}\left(\frac{kTC_s}{A}\right)^{1/2} \quad (10)$$

and the probability of a fluctuation greater than or equal to a given $\tilde{n}_c$ (of selected sign) is

$$P_c(\tilde{n}_c) = 1/2 \operatorname{erfc}\left[\frac{\Delta n}{\sqrt{2\sigma}}\right] = 1/2 \operatorname{erfc}\left[\tilde{n}\left(\frac{A}{2kTC_s}\right)^{1/2}\right], \quad (11)$$

where $\operatorname{erfc}(x)$ is the complementary error function.[1] To obtain the number of times per second that a given patch undergoes a fluctuation equal to or greater than the critical magnitude, P_c must be multiplied by the frequency of the fluctuations. This is the inverse of an average fluctuation lifetime. This frequency factor, f, is equal to the inverse of the two-dimensional random-walk diffusion time, Δt, of a lipid molecule across a patch of radius $r_m + \ell$.

$$f = \frac{1}{\Delta t} = \frac{4D_s}{(r_m + \ell)^2} = \frac{4\pi D_s}{A}, \quad (12)$$

where D_s is the diffusion coefficient of lipid molecules in the bilayer.

The number of times per second that a unit area of monolayer undergoes a fluctuation of critical or larger amplitude is then

$$N_m = \frac{1}{A} f P_c(\tilde{n}_c). \quad (13)$$

The number of critical or larger fluctuations per second occurring simultaneously in both monolayers at the same location is

$$N_b = \frac{1}{A} f P_c^2(\tilde{n}_c). \quad (14)$$

The number of events forming inverted micelles per second per unit area of membrane is then

$$N_1 = N_b F_1 = \frac{\pi D_s}{A^2}\left[\operatorname{erfc}\left\{\tilde{n}_c\left(\frac{A}{2kTC_s}\right)^{1/2}\right\}\right]^2 F_1, \quad (15)$$

where

$$F_1 = \alpha_1 \exp\left\{-\frac{G^{\neq}}{kT}\right\}\Delta t. \quad (16)$$

F_1 is the efficiency (≤ 1) with which LIP form from critically populated patches. We assume an Arrhenius rate form for F_1, with a pre-exponential factor, α_1, determined by the time scale of molecular motions and a free energy of activation $G^{\neq}$. Both of these factors depend upon the details of the molecular rearrangements accompanying the transition to micellar structure, and cannot be calculated a priori. However, we can derive estimates. The time scales of molecular displacements in liquid crystalline bilayers and H_{II} phases are in the range of nanoseconds or tens of nanoseconds (27, 42, 43). (This time scale is quite short compared with the microsecond-range duration of density fluctuations in the bilayer, so Eq. 16 is appropriate.) Thus α_1 will be roughly the inverse of this time scale, 10^8 s^{-1}.

$G^{\neq}$ is given by

$$G^{\neq} = G^{\neq}_{\text{def}} + G^{\neq}_{\text{mic}} - G_c, \quad (17)$$

where $G^{\neq}_{\text{def}}$ is the free energy of activation necessary to deform the monolayers that envelop the micelle. $G^{\neq}_{\text{mic}}$ is the free energy of activation needed to translocate lipid molecules into the bilayer interior and form the micelle. G_c is the increase in chemical potential of the lipid in the bilayer patch as a result of the critical fluctuation (due to local increase in lipid concentration). We can estimate the size of these terms.

$G^{\neq}_{\text{def}}$ is due to increases in lipid-water interfacial area and changes in the curvature of the exterior monolayers of the LIP. The interfacial tensions of phospholipid and biomembranes are quite small. In fact they are virtually tension-free in the absence of osmotic pressure gradients (44–46). Moreover, the change in lipid-water interfacial area at the LIP exterior is small. The surface area of a spherical segment of height h and base radius R is $2\pi Rh$. Here $R = r_m + \ell$ and $h = r_m$ (see Fig. 1) so the change in

[1] Values of $\operatorname{erfc}(x)$ may be obtained from tables or estimated via

$$\frac{2}{[\pi]^{1/2}}\frac{e^{-x^2}}{[x + (x^2 + 2)^{1/2}]} < \operatorname{erfc}(x) \leq \frac{2}{[\pi]^{1/2}}\frac{e^{-x^2}}{\left[x + \left(x^2 + \frac{4}{\pi}\right)^{1/2}\right]}.$$

Some approximate values of $[\operatorname{erfc}(x)]^2$ are given below

x	$[\operatorname{erfc}(x)]^2$
2	2.2×10^{-5}
3	4.9×10^{-10}
4	2.4×10^{-16}
5	2.4×10^{-24}.

exterior monolayer surface area ΔA during LIP formation is about

$$\Delta A \simeq 4\pi r_m(r_m + \ell) - 2\pi(r_m + \ell)^2 = 2\pi(r_m^2 - \ell^2). \quad (18)$$

Thus, the change in free energy due to surface creation, g_s, is $\sim g_s = 2\pi\sigma(r_m^2 - \ell^2)$, where σ is the lipid-water interfacial tension. For a tension of 0.1 dyn/cm (46) this value will be several kT or less, where k is Boltzmann's constant and T the absolute temperature. The component of $G^{\neq}_{def}$ due to the radii of curvature of the exterior monolayers is harder to estimate. This small radius of curvature will tend to pry the head groups apart, exposing more of the hydrophobic membrane interior to the aqueous phase. We can estimate this effect by an increase in apparent bilayer-water interfacial tension to some value σ'. Then $G^{\neq}_{def}$ would be approximately this value plus g_s, or

$$G^{\neq}_{def} \sim 4\pi r_m(r_m + \ell)(\sigma' - \sigma) + 2\pi\sigma(r_m^2 - \ell^2). \quad (19)$$

For $\sigma' - \sigma$ of 0.1 dyn/cm, $G^{\neq}_{def}$ would be ~5–10 kT.

$G^{\neq}_{mic}$ is hard to estimate, because it is probably a sensitive function of lipid molecule structure and of the details of the inversion process. We would expect it to be smallest for lipids that can be easily dehydrated and can create lipid-water interfaces with small radii of curvature (lipid surrounding water). These are of course the attributes of lipids that form the H_{II} phase. Further, we would expect partial lipid dehydration and micelle formation to proceed most rapidly under circumstances when this phase forms spontaneously. Thus, $G^{\neq}_{mic}$ will be smallest and LIP will form most readily when the system is very close to the lamellar-to-H_{II} phase transition. For systems that undergo a thermotropic transition, like EPE, this means that LIP can form most rapidly very close to or above the lamellar-to-H_{II} transition temperature, T_H. For systems in which cation binding drives the transition, like Ca^{+2}-CL, this means that the Ca^{+2} concentration must be above a certain critical value (24).

There is very little thermodynamic data that is applicable to an estimate of $G^{\neq}_{mic}$. Thermodynamic data for the lamellar-to-H_{II} transition are not strictly applicable because they provide equilibrium free energy differences, not activation free energies. Moreover, this transition is an interbilayer process (see section B), while LIP formation is an intrabilayer event. In the LIP case, lipid molecules must transit the monolayer, while this is probably not true of the H_{II} formation process. Free energies of dehydration (i.e., movement from the alkane-water interface to bulk alkane) have been measured for some surfactants (e.g., 47). However, these values probably represent overestimates of the values for LIP formation. They have been measured for saturated alkyl chain compounds incapable of H_{II} formation. The gain of conformational freedom of the unsaturated chains of H_{II}-forming lipids during H_{II} formation is quite marked (27), and will have a substantial entropic effect on $G^{\neq}_{mic}$. Moreover, any cooperativity in LIP formation would further reduce $G^{\neq}_{mic}$. Thus, we will assume that the product of n_m and ΔG for the lamellar-to-H_{II} transition provides a lower limit to $G^{\neq}_{mic}$, and that the product of n_m and the dehydration ΔG (several kT per molecule [47]) provides an upper limit.

The large contribution $G^{\neq}_{mic}$ makes to $G^{\neq}$ is partly offset by the increase in lipid chemical potential due to the critical concentration fluctuation, G_c. The chemical potential of the monolayer lipid is a function of the local lipid density. In the critically fluctuated monolayer patches, the area per molecule, a_c, is

$$a_c = \frac{\bar{a}}{1 + \tilde{n}_c}, \quad (20)$$

and

$$\Delta a = a_c - \bar{a} = \bar{a}\left(\frac{1}{\tilde{n}_c + 1} - 1\right). \quad (21)$$

Since C_s is given by (41)

$$C_s = \frac{-\Delta a}{\bar{a}F}, \quad (22)$$

where F is the local lateral pressure corresponding to a_c, and the free energy increase per lipid molecule, E_c, due to this compression is

$$E_c = F\Delta a, \quad (23)$$

then

$$E_c = \frac{\bar{a}}{C_s}\left(\frac{1}{1 + \tilde{n}_c} - 1\right)^2. \quad (24)$$

The total increase in free energy, G_c, of the bilayer patch undergoing a critical fluctuation is thus

$$G_c = 2(1 + \tilde{n}_c)\bar{n}E_c. \quad (25)$$

This excess free energy can be dissipated either by decay of the local concentration fluctuation (which is most frequent) or by inversion of a fraction of the lipid molecules to form a LIP. G_c can be many multiples of kT.

Note that for

$$\frac{G^{\neq}}{kT} \leq \ell n(\alpha_1 \Delta t) \quad (26)$$

F_1 will be unity.

Eq. 15 is the rate of LIP formation. The rate for reversion of LIP to bilayer structure can also be derived. In this reversion process, a critical fluctuation in the enveloping monolayers reduces the local lipid density and permits reinsertion of the molecules of the micelle into the original monolayer. The critical fluctuation magnitude in each monolayer for reversion ($\tilde{n}_{c-}$) is

$$\tilde{n}_{c-} = \frac{\Delta n}{n_e} = \frac{-n_m}{2n_e}, \quad (27)$$

where n_e is given by Eq. 6.

We can now calculate the probability of such a fluctuation as in Eq. 11. The factor of $(A/C_s)^{1/2}$ in the argument of erfc in Eq. 15 is different for the case of LIP reversion. The surface area of the exterior monolayers in the LIP is greater than the original bilayer patch area. However, the effective C_s of the LIP monolayers is probably enhanced by their small radius of curvature. The highly disordered alkyl chains of the bilayer immediately adjacent to the inverted micelle (Fig. 1) also increase the local microscopic compressibility. Reinsertion of micellar lipid into these regions is probably a much more facile process than into planar monolayers. Since the functional dependence of C_s on radius of curvature is unknown, we will simply assume that $(A/C_s)^{1/2}$ is the same as in the monolayer case. This will probably lead to an underestimate of the true reversion probability. Let P_R be the probability of a LIP reverting to bilayer structure per fluctuation lifetime. Then, as in the derivation of N_1,

$$P_R = P_c^2(\tilde{n}_{c-})F_{-1}\,. \tag{28}$$

F_{-1} is an efficiency factor similar to F_{-1}. The free energy of activation for reversion will generally be smaller than for LIP formation. Let $G_-^{\neq}$ be the free energy of activation in F_{-1}. $G_-^{\neq}$ will consist of two terms similar to the terms $G_{mic}^{\neq}$ and G_c in $G^{\neq}$. These are present because lipid molecules must still transit the monolayer and because the critical fluctuation $\tilde{n}_c$ increases the chemical potential of the monolayer lipid. The term corresponding to G_c is G_{c-}, which is given by Eq. 25, using $\tilde{n}_{c-}$ instead of $\tilde{n}_c$ and n_e instead of $\bar{n}$. E_c is given by Eq. 24, substituting $\tilde{n}_{c-}$ for $\tilde{n}_c$. Note that $|\tilde{n}_{c-}|$ is usually $>\tilde{n}_c$, and hence $G_{c-} > G_c$. Moreover, $G_-^{\neq}$ will not contain a term like $G_{def}^{\neq}$ since reversion creates no new deformation stresses (it relieves existing stresses). Therefore $G_-^{\neq}$ will be $\leq G^{\neq}$ and $F_{-1} \geq F_1$. When the inequality in Eq. 26 is violated (large $G^{\neq}$),

$$\frac{F_{-1}}{F_1} \sim \exp\left\{\frac{(G_{def}^{\neq} + G_{c-} - G_c)}{kT}\right\}. \tag{29}$$

The steady state number of LIP per unit area, n_{LIP}, is obtained from

$$\frac{dn}{dt}\,\text{LIP} = 0 = N_1(1 - An_{LIP}) - k_R n_{LIP} \tag{30}$$

where N_1 is given by Eq. 15 and k_R is the rate constant for LIP reversion,

$$k_R = P_R/\Delta t\,. \tag{31}$$

P_R is given by Eq. 28 and Δt by Eq. 12. Using Eqs. 30 and 31,

$$n_{LIP} = \left(A + \frac{k_R}{N_1}\right)^{-1}. \tag{32}$$

From Eqs. 15, 28, and 31,

$$\frac{k_R}{N_1} = A\left(\frac{F_{-1}}{F_1}\right)\left[\frac{P_c(\tilde{n}_{c-})}{P_c(\tilde{n}_c)}\right]^2 \tag{33}$$

and

$$n_{LIP} = \left(A\left\{1 + \left(\frac{F_{-1}}{F_1}\right)\left[\frac{P_c(\tilde{n}_{c-})}{P_c(\tilde{n}_c)}\right]^2\right\}\right)^{-1}. \tag{34}$$

Close to the lamellar-to-H_{II} transition, $n_{LIP} \sim 1/A$, since $P_c(\tilde{n}_{c-})$ is usually $\ll P_c(\tilde{n}_c)$.

Far from the lamellar-to-H_{II} transition, when the system is more stable in the lamellar phase, $G^{\neq}$ becomes much larger than $G_-^{\neq}$. (Far below T_H, for example, the alkyl chains of the lipid cannot adopt the more disordered configuration in the H_{II} phase.) In this limit

$$n_{LIP} \sim \frac{1}{A}\left[\frac{P_c(\tilde{n}_c)}{P_c(\tilde{n}_{c-})}\right]^2 \exp\left[(G^{\neq} - G_-^{\neq})/kT\right]. \tag{35}$$

Steady state LIP density should therefore decrease rapidly as the stability of the bilayer phase increases.

Four things should be noted concerning the large steady state LIP density predicted by Eq. 34. First, it is achieved quite slowly. An estimate of the time, t_n, required is

$$t_n > \frac{n_{LIP}}{N_1} \sim 2/f P_c^2(\tilde{n}_c)F_1\,. \tag{36}$$

P_c^2 is such a small quantity that t_n is a macroscopically long interval. Second, Eq. 34 overestimates n_{LIP}. As noted previously, $P_c^2(\tilde{n}_{c-})$ is probably much larger than the value calculated using monolayer values of C_s. This is true because disorder in the monolayers immediately adjacent to the inverted micelle and in the highly curved exterior monolayers probably increases the local value of C_s. Even a 10% increase in the effective C_s would increase $P_c^2(n_{c-})$ three to 30-fold for typical values of the argument of erfc(x). This would decrease n_{LIP}. Third, when the inequality in Eq. 26 is violated and $G^{\neq}$ is large, (F_{-1}/F_1) becomes $\gg 1$ (Eq. 29). This greatly reduces n_{LIP}: for $G^{\neq} - G_-^{\neq} = 5$ kT, $(F_{-1}/F_1) = 148$. Finally, at large n_{LIP}, the LIP probably aggregate into strings, forming structures resembling H_{II} rods enveloped by monolayers (3, 8). This is energetically favorable, since aggregation increases one principal radius of curvature at each of the lipid-water interfaces in the LIP.

We can also estimate the half-life $t_{1/2}$ of a LIP. The LIP reversion probability per unit time is $P_R/\Delta T$ and we obtain $t_{1/2}$ via

$$0.5 = \int_0^{t_{1/2}} \frac{P_R}{\Delta t}\,dt\,. \tag{37}$$

P_R is time independent and is zero for $t = 0$. Δt is a constant, so

$$t_{1/2} = \frac{\Delta t}{2P_R} = 2\left\{\text{erfc}\left[\tilde{n}_{c-}\left(\frac{A}{2kTC_s}\right)^{1/2}\right]\right\}^{-2}\frac{\Delta t}{F_{-1}}. \tag{38}$$

Note that if $n_e = \tilde{n}$ ($\tilde{n}_{c-} = \tilde{n}_c$) then

$$(\tilde{n}_{c-} = \tilde{n}_c)\colon t_{1/2} = t_n\,. \tag{39}$$

We can now estimate n_{LIP}, N_l, and $t_{1/2}$ for an egg phosphatidylethanolamine (EPE) bilayer. Lipidic particles are often observed in such unsaturated PE preparations (e.g., 3, 8, 15). We use bilayer dimensions and lateral compressibility data at 25°C from (41), and area per head group data from references 41 and 48. Since T_H for EPE is ~30°C (23), these values are relevant to the correct temperature range. The thickness of the bilayer (=2ℓ) is ~4 nm (41). The diameter of H_{II} rods in natural PE systems is 6–8 nm (3, 48–50). Using this diameter (7.0 nm) as the diameter of the inverted micelle (equals 2 r_m) yields a diameter for the monolayer-enveloped structure of 11.0 nm. This value is compatible with observations of the size of lipidic particles (~10 nm, [8]).

The area per headgroup, a_0, at the lipid-water interface in the H_{II} phase is 0.42 nm^2 (48). We thus find

$$n_m = \frac{4\pi(r_m - \ell)^2}{a_0} = 67 \text{ molecules.} \quad (40)$$

With this result, using Eqs. 1 and 5, we find

$$\tilde{n}_c \simeq 0.248.$$

We use a value of 0.067 cm/dyn for C_s (41) and $D_s = 3 \times 10^{-8}$ cm^2/s, which is appropriate for liquid crystalline bilayers of unsaturated phospholipids (51, 52).

N_l, n_{LIP}, $t_{1/2}$, and t_n will be in terms of F_l and F_{-l}. We can estimate F_l using Eq. 15. We take $\alpha_l = 10^8$ and calculate $\Delta t = 2.5$ μs via Eq. 12. Then $F_l = 250 \cdot \{\exp(-G^{\neq}/kT)\}$. According to Eq. 26, if $G^{\neq} \leq 5.5$ kT, F_l will equal 1. By Eqs. 23 and 24 we calculate $G_c \simeq 38$ kT. Since $G^{\neq}_{def}$ is probably only several kT, $F_l = 1$ for $G^{\neq}_{mic} \lesssim 38$ kT, or $38/n_m = 0.6$ kT per lipid molecule forming the micelle. This energy is large compared with the free energy ΔG_H of the lamellar-to-H_{II} transition, and small compared with values estimated using dehydration energies. The enthalpy ΔH_H of the transition in EPE is ~0.5 kT per molecule (27). Within a few degrees of T_H, ΔG_H is given by

$$\Delta G_H = \Delta H_H\left(1 - \frac{T}{T_H}\right). \quad (41)$$

For $T_H - T = 5°$, ΔG_H is <0.01 kT per molecule. By comparison, free energies of dehydration of simple fatty acids are quite large (~4 kT, [47]). This would yield a $G^{\neq}_{mic}$ of ~270 kT, which would make F_l and N_l effectively zero. Therefore, we assume a value of 38 kT for $G^{\neq}_{mic}$ to make $F_l \rightarrow 1$, and treat the results as upper limits on N_l and n_{LIP}.

Using $F_l = F_{-l} = 1$, we obtain (Eqs. 15, 34, 36, 39) $N_l \lesssim 90$ LIP/μm^2/h; $n_{LIP} \lesssim 1/A \sim 10^4/\mu$m^2, $t_{1/2} \lesssim 2{,}000$ h, and $t_n > 100$ h. These values are upper limits (N_l, $t_{1/2}$, n_{LIP}) and a lower limit (t_n) on the anticipated values, respectively. LIP are predicted to form very slowly, if at all, in this system. The half-life of those that do form is predicted to be quite long, and the steady state LIP density would be achieved only after many days of incubation. These results are qualitatively compatible with the reported absence of lipidic particle structures in unilamellar EPE vesicle preparations (17).

We emphasize that the values derived above are upper bounds on N_l and n_{LIP}. If $G^{\neq}_{mic}/n_m$ were only 1 kT, as apposed to the value of 0.6 kT assumed above to make $F_l = 1$, N_l would be 2×10^{-10} LIP/μm^2/h. For all practical purposes, LIP could not form. Likewise, we use a value of C_s of 0.067 cm/dyn (41). This is almost an order of magnitude larger than typical values from vesicle deformation experiments (53, 54). A value only 20% smaller would reduce N_l by a factor of two hundred. LIP would be so rare as to evade detection via electron microscopy.

To calculate N_l, n_{LIP}, $t_{1/2}$, and t_n for the Ca^{+2}-CL system, we use $a_0 = 0.584$ nm^2 and $r_i = 0.75$ nm (55). The H_{II} rod diameter is 5.3 nm (55). We assume that this diameter equals $2r_i + 2\ell$, yielding $\ell = 1.9$ nm. Measurements of $\bar{a}$ in bilayers in the presence of Ca^{+2} are lacking. We use Rand and Sengupta's estimate (55) of 1.2 nm^2/molecule. Measurements of C_s in bilayers or monolayers at the oil/water interface are also lacking. We use the value of 0.010 cm/dyn determined in monolayers at the air/water interface (56–58). We assume that $G^{\neq}_{mic}$ is ~1 kT per lipid phosphate group in the micelle, and that $G^{\neq}_{def}$ is 5 kT. We calculate $G_c = 1.2$ kT via Eqs. 24 and 25. At 25°C and with $D_s = 3 \times 10^{-8}$ cm^2/s, we find $N_l \leq 250$ LIP/μm^2/h; $n_{LIP} \leq 1/A = 1.5 \times 10^4$ LIP/μm^2, $t_{1/2} < 4$ y, and $t_n > 60$ h. Using freeze-fracture electron microscopy, others (19) have observed lipidic particles in 0.2 μm-diameter unilamellar CL-PC vesicles (in the absence of cryoprotectant) only after hours of incubation in the presence of Ca^{+2}. This is roughly compatible with the value of N_l given above. At that rate, LIP would constitute 1% of the surface area of a 0.2 μm-diameter vesicle of pure CL after 0.6 h. The rate of appearance of LIP would be slower in a mixed CL-PC system (see the following parts entitled Formation of LIP in Two-Component Systems and Conclusions Concerning the LIP Model).

As with EPE, these numbers are upper bounds (N_l, n_{LIP}, $t_{1/2}$) and a lower bound (t_n), respectively. Note that $G^{\neq}$ is large (~28 kT) for Ca^{+2}-CL, and $F_l \ll 1$. In this system, our assumptions about $G^{\neq}$ control the value of N_l. Our assumption that $G^{\neq}_{mic}$ is only 1 kT/phosphate group (2/CL molecule) in the micelle is conservative. For simple molecules like alkanols, the free energy of dehydration is four times kT around room temperature (47). Even when complexed with Ca^{+2}, the phosphate groups should be somewhat hydrophilic, and there is an additional exposed hydroxyl group on the CL head group. If $G^{\neq}_{mic}$ were increased 20%, N_l would be reduced 100-fold. Thus, as with EPE, we conclude that LIP form very slowly in Ca^{+2}-CL systems, if at all. The results are compatible with observations of unilamellar CL-containing systems.

The physical relevance of these calculations will be further discussed in the final part of this section. Note that these expressions are very sensitive to input parameters.

For typical values of the argument of erfc(x) (x = 2 to 4), a 10% change in x produces a difference of about three to 30-fold in erfc(x), respectively. The equations can only be relied on for order-of-magnitude estimates.

Several assumptions have been made to make the theory tractable. First, we have assumed that fluctuations in the two monolayers of the bilayer are independent. As outlined in the beginning of this section, this is probably reasonable if the two alkyl chains of each lipid molecule are of about equal length. Second, we have assumed that C_s is independent of the local lipid concentration. This will probably break down for high local lipid concentrations (i.e., $\tilde{n}_c \gtrsim 0.1$), making the calculated N_1 values overestimates of the true rates. Third, we have used a simplistic model to derive the inverted micellar dimensions. Because of more severe head group packing constraints at the spherical interface in the micelle, for example, it is probable that r_i is greater than or equal to the radius of the H_{II} water channel. Again, this would lead to an overestimate of N_1.

Finally, it may be objected that it is inappropriate to use a well-defined C_s at or near the lamellar-to-H_{II} transition because of the compressibility divergence in the neighborhood of phase transitions involving molar volume changes. This is not the case for LIP formation in isolated bilayers (e.g., in unilamellar vesicles). There does not seem to be an accessible pathway to H_{II} phase formation until several bilayers are apposed to one another ([8] and section B). LIP, if they exist, are not thermodynamically stable structures (due to the unfavorable small radii of curvature of the enveloping monolayers) and form very slowly: therefore, they do not produce such divergence close to T_H.

Formation of LIP in Two-Component Systems

Consider a bilayer containing component No. 1, an H_{II}-forming lipid, and component No. 2, which only exists in the lamellar phase under the ambient conditions. If component No. 2 cannot participate in LIP formation, we presume that concentration fluctuations in the bilayer cannot lead to LIP formation unless large enough patches of pure component No. 1 are formed. For simple systems, one can easily calculate this demixing probability, P_D.

We make several assumptions. First, the lipids must form ideal mixtures. Second, we assume that the areas per molecule in the bilayer are equal for both species,

$$\bar{a}_1 = \bar{a}_2 = \bar{a}. \tag{42}$$

Finally, the fluctuations in lipid concentration in a monolayer are assumed to be nearly symmetrical. The surpluses of the components are in the same ratio as their bulk concentrations. This is a good approximation if the mole fraction of either component is not too small and the total number of molecules in A is large.

The equation for the LIP formation rate in the two-component system is

$$N_2 = \frac{\pi D_m}{A^2}\left\{\text{erfc}\left[\tilde{n}\left(\frac{A}{2kTC_m}\right)^{1/2}\right]\right\}^2 P_D^2 F_1. \tag{43}$$

C_m and D_m are the compressibility and lipid diffusion coefficient, respectively, in the mixture. A will be the same as in the one-component case. P_D is the probability that a critically fluctuated monolayer patch of area A forms a region of $n_m/2$ molecules of pure component No. 1.

P_D is obtained via simple combinatorial formulae for the partition functions of the original mixture (patch undergoing a critical fluctuation, before demixing) and the demixed system. Let x_1 and x_2 be the mole fractions of the components. Using the combinatorial formula for distributing n indistinguishable objects so that $\{n_i\}$ objects are in the categories $\{i\}$, we find the partition function for the original mixture is

$$\Omega_m = \left\{\left(\frac{n_m x_i}{2}\right)!\left[\left(n - \frac{n_m}{2}\right)x_i\right]!\left[(1-x_1)\frac{n_m}{2}\right]!\left[\left(n - \frac{n_m}{2}\right)(1-x_i)\right]!\right\}^{-1} \tag{44}$$

and the corresponding expression for the partially demixed system is

$$\Omega_D = \left\{\left(\frac{n_m}{2}\right)!\left[\left(n - \frac{n_m}{2x_1}\right)x_1\right]![1-x_1)n]!\right\}^{-1}. \tag{45}$$

The entropy of demixing, S_D, and free energy of demixing, ΔG_D, are

$$\Delta S_D = k \ln \Omega_D - k \ln \Omega_m = k \ln\left[\frac{\Omega_D}{\Omega_m}\right], \tag{46}$$

and

$$\Delta G_D = -kT \ln\left[\frac{\Omega_D}{\Omega_m}\right], \tag{47}$$

and the probability of demixing is

$$P_D = \exp\{-\Delta G_D/kT\} = \frac{\Omega_D}{\Omega_m}. \tag{48}$$

The expression for P_D thus becomes

$$P_D = \frac{\left(\frac{n_m x_1}{2}\right)!\left[\left(n - \frac{n_m}{2}\right)x_1\right]!\left[(1-x_1)\frac{n_m}{2}\right]!\left[\left(n - \frac{n_m}{2}\right)(1-x_1)\right]!}{\left(\frac{n_m}{2}\right)!\left[\left(n - \frac{n_m}{2x_1}\right)x_1\right]![(1-x_1)n]!}, \tag{49}$$

where $n = n_e + n_m/2$. The expression for the rate of reversion N_{-2} of inverted micelles per unit area in this system is identical to N_{-1} except for the use of C_{sm} and D_{sm}.

The expression for n_{LIP} becomes (for $F_1 = F_{-1} = 1$)

$$n_{LIP} = A^{-1}\left\{1 + \left[\frac{P_c(\tilde{n}_{c-})}{P_c(\tilde{n}_c)}\right]^2 \left(\frac{F_{-1}}{F_1}\right)(P_D)^{-2}\right\}^{-1}. \quad (50)$$

P_D^2 decreases rapidly with increasing x_2. For systems like EPE, $x_2 > 0.10$ should greatly reduce the LIP formation rate, N_2. Some values of P_D^2 for EPE mixed with a lamellar phase impurity are given below ($n = 159$, $n_m/2 = 34$, $a_{EPE} = a_2 = 0.75$ nm^2, from the first part entitled One-Component Systems).

x_2	P_D^2
0.05	0.20
0.10	0.062
0.15	7.3×10^{-5}
0.20	7.8×10^{-7}.

The ratio N_2/N_1 is proportional to P_D^2. However, the presence of component No. 2 will make $C_m \neq C_s$, which will also substantially affect N_2/N_1. A first order approximation for C_m would be to use the sum of the products of the compressibilities of each component with the mole fraction of that component.

If the mixture is at all nonideal, Eq. 49 will underestimate the true P_D. Any tendency of the components to self-associate can make $G_D \leq 0$. For example, at $x_2 = 0.20$ in the example above, G_D is only 7 kT for a separation of 34 EPE molecules. If the self-association free energy of EPE is as small as 0.2 kT/molecule, $G_D \sim 0_s$ and $P_D \rightarrow 1$. (Conversely, EPE-impurity affinity would raise G_D and lower P_D.)

Note, however, that it might not be necessary to form a single patch of $n_m/2$ component No. 1 molecules. First, inversion may be possible from a number of smaller patches. Second, there are reports (e.g., 26, 59) that the ^{31}P-NMR spectra of non-H_{II}-forming phospholipids contain an isotropic component when the phospholipids are part of a lipidic particle-forming mixture. The non-H_{II}-forming phospholipid head groups are subject to some sort of isotropic motional averaging. This may arise from motion around the water cavity in the micelle or around the highly curved exterior monolayers of the LIP (or IMI, see section B). If the former effect is the cause of the isotropic signal, it would indicate that extensive demixing of critically fluctuated patches of bilayer is unnecessary. This would make Eq. 43 a serious underestimate of N_2.

Conclusions Concerning the LIP Model

The calculations in the preceding parts show that

(*a*) LIP should be rare, if they exist at all. Using optimistic assumptions about r_i and $G^{\neq}_{mic}$, the model predicts that unilamellar EPE preparations at or very near T_H should form LIP at a maximum rate of 90 LIP per square micron of membrane per hour. The predicted maximum rate for Ca^{+2}-CL using $G^{\neq}_{mic}/n_m \sim 2\ kT$ (at 25°C at or near the $[Ca^{+2}]$ threshold for H_{II} formation) is 250 LIP/μm^2/h. Slightly less optimistic assumptions about r_i, C_s, and $G^{\neq}_{mic}$ reduce these formation rates by several orders of magnitude. These results are consistent with the absence of lipidic particle morphology in unilamellar EPE preparations (17) and near absence in unilamellar Ca^{+2}-CL-PC preparations (incubated without cryoprotectant [19]).

(*b*) The predicted steady state LIP densities are very large, resulting in closely packed arrays of LIP. These densities are large overestimates since reversion rates are probably seriously underestimated by the model. The steady state is achieved quite slowly (days to weeks). The slow accumulation of LIP is qualitatively compatible with the long incubation times (hours) necessary before any lipidic particle morphology appears in unilamellar Ca^{+2}-CL-PC preparations (19).

(*c*) The predicted half-lives of LIP are also quite long (months or longer). Once again, as discussed in the part entitled One-Component Systems, these are overestimated by the model. Qualitatively, these results are compatible with the pronounced hysteresis of lipidic particle morphology and isotropic ^{31}P-NMR spectra (6, 26, 60, 61).

(*d*) The LIP formation rate should decrease rapidly when mixed with increasing amounts of a non-H_{II}-forming component.

(*e*) LIP are not thermodynamically stable. Their formation and reversion rates are just very small.

In comparing these predictions to experiment, I have emphasized observations on unilamellar lipid preparations as opposed to multilamellar preparations. This is an important distinction. Large numbers of lipidic particles are observed in multilamellar lipid preparations quenched after incubation above the lamellar-to-H_{II} phase transition (e.g., 3, 6, 12, 17), while very few are observed in unilamellar preparations. In unilamellar preparations, apposition of two vesicle membranes can be a comparatively rare event, while this situation is ubiquitous in liposomes. This suggests two possibilities. The first is that different lipidic particle structures form in each case, the structure in the unilamellar case arising from an intrabilayer event (i.e., a LIP) and the structure in liposomes from an interbilayer event. Alternatively, the lipidic particle structures in unilamellar preparations may be of the interbilayer type, their reduced frequency resulting from the infrequent close apposition of vesicles. Interbilayer structures will be examined in the next section.

The present model shows that LIP structures may form at rates slow enough to be compatible with observations from unilamellar systems, i.e., they may be a good model for the intrabilayer structure described above. However, it remains to be demonstrated that these lipidic particle images are LIP. Careful freeze-fracture electron micrographic studies of vesicle preparations are required. A LIP (i.e., intrabilayer) model of lipidic particles is applicable only if these structures are found on unilamellar vesicles

outside of regions of vesicle–vesicle contact. The predicted formation rates of LIP are quite slow. LIP might escape detection unless large areas of unilamellar structure interface are examined after lengthy incubation near the lamellar-to-H_{II} transition. The latter requirement means that care must also be taken to either limit vesicle aggregation or rigorously exclude lipidic particle images present on planes of vesicle–vesicle apposition.

LIP structures will only form in lipid systems with compounds that can adopt the H_{II} phase near the lamellar-to-H_{II} transition. Systems with the following attributes will have the best chance of evolving LIP at observable rates: (*a*) H_{II} rod dimensions $\bar{a}$, a_0, and ℓ such that

$$\tilde{n}_c = \left| \frac{(n_m + 2n_c)}{2\bar{n}} - 1 \right| \ll 1 ,$$

where n_m, n_c, and $\bar{n}$ are given by Eqs. 1, 3, and 4, respectively; (*b*) $G^{\neq}_{mic} \lesssim n_m\, kT$ (this is most likely in systems with easily dehydrateable head groups, very close to the lamellar-to-H_{II} transition of the bulk lipid-water system); (*c*) large lateral compressibility C_s, especially if $\tilde{n}_c > 0.1$. Note that G_c is proportional to C_s^{-1}; Eqs. 24, 25. A large C_s is desirable to increase P_c (Eq. 11) provided that the simultaneous decrease in G_c does not make $G^{\neq}$ too large (Eqs. 16, 17). (*d*) In mixed systems, the mole fraction of H_{II}-forming component should be large ($\gtrsim$0.8). This will not be important in systems where the mixture is nonideal or where external influences (e.g., multivalent cation binding in charged lipid systems) induce lateral phase separations.

B. FORMATION OF IMI BETWEEN APPOSED BILAYERS

Theory

IMI Formation Rate. We assume that IMI are structures similar to those depicted in references 15 and 61. This structure is shown in Fig. 2 *a*. IMI formation is treated as a three-step process. First, two bilayers are closely apposed, so that the monolayers are <1-nm apart. This allows the motions of molecules in the facing monolayers to become coordinated. Because phospholipid membranes repel each other at these small separations (62–64) this is not necessarily a frequent occurrence. Second, the lipid concentration in the apposed monolayers must be sufficient to form an IMI structure. A major difference between IMI formation and LIP formation (section A is that the equilibrium lipid concentration is usually sufficient to form the inverted micellar structure. This greatly increases the anticipated overall formation rate, since large fluctuations in lipid concentration are rare. Third, if a sufficient free energy of activation energy is available, the lipids in the apposed monolayers will rearrange into the IMI configuration (Fig. 2 *a*). The probability of IMI formation by this third process is the product of an

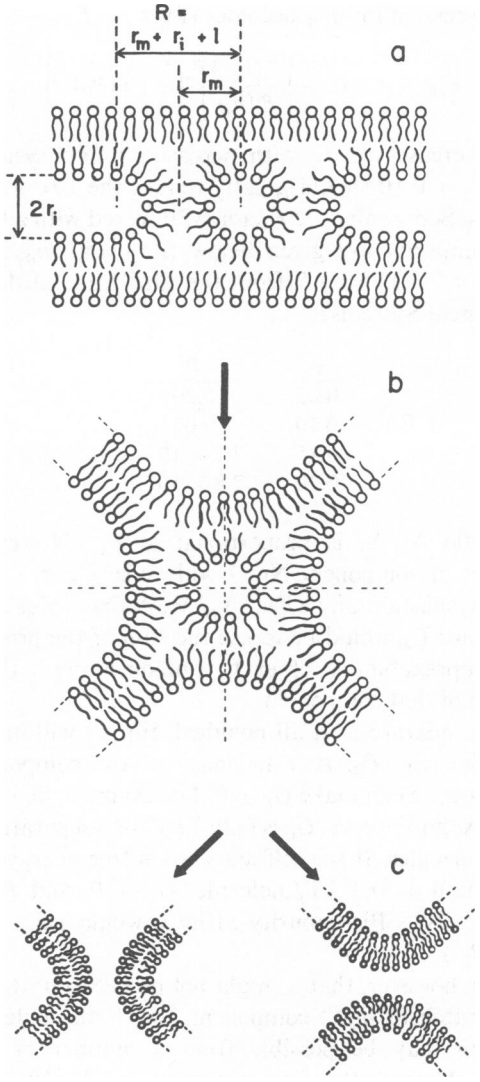

FIGURE 2 (*a*) IMI structure in cross section. The inverted micelle is spherical. The structure is cylindrically symmetrical about the vertical axis (dashed line through the center of the micelle). (*b*) Rearrangement of the bilayer attachments to the IMI. The structure is still cylindrically symmetrical about the vertical axis. (*c*) Products of IMI reversion to bilayer structures. *Left:* fusion of the two original lamellae, resulting from rearrangement of the micellar lipid around the vertical axis of *b*. *Right:* re-formation of original lamellae, resulting from rearrangement about the horizontal plane of symmetry (dashed horizontal line in *b*).

Arrhenius rate constant and a fluctuation lifetime, as in LIP formation. The free energy of activation for this process is probably much smaller than in the LIP case, however. Lipid molecules do not have to be totally dehydrated and travel through a monolayer to form the inverted micelle. Part of the water-lipid interface of the apposed monolayers becomes the water-lipid interface in the micelle.

The IMI can revert to bilayer structure by re-formation of the original planar membrane interfaces. When this occurs, either the original two membranes are re-formed (Fig. 2 *c*, right) or the two original membranes are made

continuous (Fig. 2 *c*, left); this latter process is membrane fusion. Note that in the final stage of the fusion process, the site of the IMI will resemble a cusplike interbilayer attachment. This may be the origin of the cusps observed in freeze-fracture electron micrographs of liposomes near the lamellar-to-H_{II} phase transition (e.g., 12, 17).

First, we calculate the number of lipid molecules in an IMI. The structure in Fig. 2 *a* consists of a spherical inverted micelle (radius $r_m = r_i + \ell$) inside an annular interbilayer attachment. This annulus is a semitorroidal monolayer of lipid. The surface area (SA) of this semitorroidal region is then

$$SA = 2\pi^2 r_i(r_m + \ell + r_i) - 4\pi r_i^2 . \quad (51)$$

The principal radii of curvature of this surface are r_i and $r \geq r_m + \ell$. The former is the radius of the water cavity of the micelle (approximately the radius of the water channel in the H_{II} phase), and the latter is somewhat smaller than the limiting radii of small sonicated lipid vesicles (65, 65*a*). The area per lipid head group, a', on this surface will be intermediate between the areas appropriate for each of these radii, i.e.,

$$a' = \sqrt{a_0}\sqrt{\bar{a}} . \quad (52)$$

The number of molecules in the semitorroidal monolayer is then simply SA/a'. The number of molecules in the micelle, n_m, is calculated (for a given r_i) as in section A (Eq. 1).

We proceed by calculating the probability of fluctuations large enough to assemble the number of molecules necessary to form an IMI. The area of the original monolayer patches that form the IMI is

$$A = \pi(r_m + \ell + r_i)^2 . \quad (53)$$

$\bar{n}$, the number of molecules in a patch of this area at equilibrium, is given by

$$\bar{n} = A/\bar{a} . \quad (54)$$

The number of lipid molecules in an IMI is then

$$n_b = \frac{SA}{a'} + n_m . \quad (55)$$

The scaled magnitude of the critical fluctuation, $\tilde{n}_c$, in each facing monolayer of the apposed bilayers is

$$\tilde{n}_c = \frac{(n_b/2) - \bar{n}}{\bar{n}} , \quad (56)$$

which, using Eqs. 53–56, becomes

$$\tilde{n}_c = \left[\frac{\pi r_i(r_i + \ell) + r_i^2[(\bar{a}/a_o)^{1/2} - 1]}{2(r_i + \ell)^2}\right]\left(\frac{\bar{a}}{a_0}\right)^{1/2} - 1 . \quad (57)$$

In calculating the magnitude and probability of the critical fluctuations, we have to distinguish between two limiting situations. The fluctuations in the exterior leaflets of the two bilayers could be almost independent (uncoupled) at small interbilayer separations. Alternatively, if the interbilayer separation is quite small or multivalent cations form intermembrane complexes between lipid head groups, the fluctuations might be coupled. Motions of molecules in one monolayer would be strongly influenced by the motion of molecules in the other. This may well be the case in some charged phospholipid-divalent cation H_{II}-forming systems (e.g., Ca^{+2}-cardiolipin [55] and Ca^{+2}-phosphatidic acid [4]).

We can calculate the probability of the critical fluctuations in both of these cases. We assume that the coupled limit corresponds to formation of bimolecular intermembrane lipid complexes. In this case, it is the number of lipid complexes within area A that fluctuates, and not the number of individual lipid molecules in each facing monolayer, as in the uncoupled limit. In the coupled limit, a critical fluctuation is one that assembles $n_b/2$ bimolecular complexes within area A. The equilibrium number of complexes within area A is simply $\bar{n}$, the equilibrium number of lipid molecules in each monolayer. Thus, $\tilde{n}_c$ in the strong-coupling case is the same as the value given by Eq. 55, which is $\tilde{n}_c$ for the uncoupled limit.

In the coupled limit, the number of times per second that critical or larger fluctuations occur in a 1-cm^2 patch of two closely apposed bilayers is given by an expression analogous to Eq. 13 in section A

$$N_m = \frac{1}{A} f P_c(\tilde{n}_c), \quad (58)$$

where

$$P_c(\tilde{n}_c) = \frac{1}{2}\operatorname{erfc}\left[\tilde{n}_c\left(\frac{A}{2kTC_s}\right)^{1/2}\right] \quad (59)$$

$$f = 4\pi D_c/A. \quad (60)$$

(Naturally, A and $\tilde{n}_c$ are now the values calculated for IMI, Eqs. 53 and 56, respectively.) The number of IMI formed per second per unit area between two bilayers apposed in the coupled limit is

$$N_{3c} = N_m F_3 P_a = \frac{2\pi D_c}{A^2}\left\{\operatorname{erfc}\left[\tilde{n}_c\left(\frac{A}{2kTC_s}\right)^{1/2}\right]\right\} F_3 P_a . \quad (61)$$

P_a is the fraction of the time that the interfaces spend closely apposed. This is a function of the geometry and size of the interacting bilayer structures (e.g., liposomes, vesicles) and the forces acting between them. F_3 is an efficiency factor similar to F_1 (Eq. 16, section A). D_c is the lateral diffusion coefficient of the bimolecular complex. The membrane interiors are probably a much more viscous environment than the intervening aqueous phase. Thus, D_c is primarily a function of the size of the diffusing entity's hydrophobic moiety. According to Saffman's (66) expression, if D_s is the diffusion coefficient of a single lipid molecule, $D_c \approx D_s/2$.

In the uncoupled limit, the frequency of fluctuations greater than or equal to the critical fluctuation in a unit area patch of closely apposed bilayers is given by an expression like Eq. 14

$$N_b = \frac{1}{A} f P_c^2(\tilde{n}_c). \tag{62}$$

The frequency of IMI formation per unit area of apposed bilayer in the uncoupled limit is

$$N_{3u} = N_b F_3 P_a = \frac{\pi D_s}{A^2}\left\{\text{erfc}\left[\tilde{n}_c\left(\frac{A}{2kTC_s}\right)^{1/2}\right]\right\}^2 F_3 P_a, \tag{63}$$

where A and $\tilde{n}_c$ assume the values calculated via Eqs. 53 and 56. Note that N_{3u} contains an additional factor of $P_c(\tilde{n}_c)$, which should reduce it relative to N_{3c}.

In section A, we noted that r_i was at least as large as the radius of the water rods in the H_{II} phase. It is probably larger due to the more severe head group packing constraints at a spherical interface. In the LIP case, increasing r_i always increases $\tilde{n}_c$, reducing the LIP formation rate. It is very important to note that this is not true for IMI. A real value of r_i always exists such that $\tilde{n}_c = 0$, and this value is usually only slightly larger than the H_{II} water rod radius. This value, r_0, is found by setting $\tilde{n}_c = 0$ in Eq. 57 from which

$$r_0 = \frac{-B \pm (B^2 - 8A\ell^2)^{1/2}}{2A}, \tag{64}$$

where $A = 2 - b(\pi + b - 1)$, $B = \ell(4 - \pi b)$, and $b = (\bar{a}/a_0)^{1/2}$. Naturally, one takes the positive real value as the physically significant one. For $r_i = r_0$, $\tilde{n}_c = 0$, and $P_c(\tilde{n}_c) = 1$. The lipid concentration in the apposed monolayers is thus always appropriate for IMI formation, and the formation rate is limited by P_a and F_3. It is possible that r_i may be somehow constrained to be different from r_0. In such cases, Eqs. 61 or 63 are appropriate for N_{3c} or N_{3u}. We will assume that $r_i = r_0$ if r_0 is no more than a few tenths of a nanometer larger than the H_{II} rod diameter. (For r_0 greater than this, n_m becomes so large that very extensive cooperative motions are necessary to form the micelle. Moreover, the conformational freedom of the alkyl chains in the micelle is reduced relative to the H_{II} phase if r_i becomes too large. Both effects reduce F_3 considerably.)

For $r_i = r_0$ Eqs. 61 and 63 both reduce to

$$N_3 = \left(\frac{\alpha_1}{A}\right)\exp\{-G^{\neq}/kT\}P_a, \tag{65}$$

where we have used $F_3 = (\alpha_1/f)\exp\{-G^{\neq}/kT\}$ in analogy to Eq. 16.

One could also write an expression for the effect of non-H_{II}-forming impurities on N_3, N_{3u}, or N_{3c}. The expression for P_D would be the same as Eq. 49, using the IMI values for n_m and $\bar{n}$ (Eq. 54). This approximation assumes ideal mixing and is subject to all the possible effects mentioned in section A under Formation of LIP in Two-Component Systems. N_{3u} would include a factor of P_D^2 and N_{3c} a factor of P_D.

We assume that $G^{\neq}$ is a sum of three components G_c, $G_{def}^{\neq}$, and $G_{mic}^{\neq}$ as in section A,

$$G^{\neq} = G_{mic}^{\neq} + G_{def}^{\neq} - G_c. \tag{66}$$

G_c is obtained via

$$G_c = 2(1 + \tilde{n}_c)\bar{n}E_c \tag{67}$$

in analogy to Eq. 25, where E_c is obtained via Eq. 24 using the IMI values of $\tilde{n}_c$. If $r_i = r_0$, then E_c and G_c are 0 because $\tilde{n}_c = 0$.

$G_{def}^{\neq}$ is the free energy of activation necessary because of the change in total lipid-water interfacial area during IMI formation (g_s) and the change in curvature of the monolayers surrounding the inverted micelle. (The changes in curvature at the micellar lipid-water interface are accounted for in $G_{mic}^{\neq}$.) The total change in lipid-water interfacial area, ΔA, is

$$\Delta A = SA + 4\pi r_i^2 - 2A \tag{68}$$

and the component of $G_{def}^{\neq}$ due to area changes, g_s, is

$$g_s = \sigma \Delta A, \tag{69}$$

where σ is the average lipid-water interfacial tension. As in the first part of section A entitled One-Component Systems, we assume that the effect of curvature can be accounted for by an increase in the effective interfacial tension to some greater value, σ'. Then,

$$G_{def}^{\neq} = g_s + (\sigma' - \sigma)(SA) = \sigma'(SA) - \sigma(2A - 4\pi r_i^2). \tag{70}$$

For $\sigma = 0.1$ dyn/cm and $\sigma' = 2\sigma$ (as in section A, One-Component Systems), $G_{def}^{\neq}$ will be in the range of 1–2 kT.

$G_{mic}^{\neq}$ is the free energy of activation needed to form the inverted micelle. It is probably a sensitive function of lipid molecule structure and of the sorts of molecular displacements involved in micelle formation. As with LIP, we would expect $G_{mic}^{\neq}$ to decrease as the system approaches the lamellar-to-H_{II} phase transition. However, $G_{mic}^{\neq}$ for IMI formation is probably much smaller than for LIP formation. To form the micelles in IMI, n_m lipid molecules do not have to be largely dehydrated and pass through a lipid monolayer. The existing lipid-water interfaces of the apposed monolayers can become the lipid-water interface in the micelle.

We can only crudely estimate $G_{mic}^{\neq}$ for IMI because we don't know the details of the micelle formation process. A lower limit to $G_{mic}^{\neq}$ is certainly n_m multiplied by the free energy difference between the lamellar and H_{II} phases when the micelle forms. A more reasonable estimate can be made only by making some intelligent guesses about the IMI formation process. It seems reasonable to assume that the inverted micelle forms from two regions on the apposed

membranes, each containing $\sim n_m/2$ molecules. If the two circular regions are pressed closely together around their peripheries, the two lipid-water interfaces can merge to form the spherical interface in the inverted micelle (see Fig. 3). The number of molecules on the periphery of a circular monolayer region containing $n_m/2$ molecules is $(2\pi n_m)^{1/2}$. $G^{\neq}_{mic}$ will be roughly this number times the free energy per molecule of the process occurring at the periphery of the regions. This process probably involves simultaneous disruption of head group-head group interactions in the planes of the monolayers, development of such interactions between head groups in the apposed interfaces, and changes in the conformation of the alkyl moieties tending to decrease the interfacial radius of curvature. Since the lipid head groups do not have to be thrust into hydrophobic domains for this to occur, the required free energy of activation will be much smaller than $G^{\neq}_{mic}/n_m$ in the LIP case. For LIP, we assumed (section A) $G^{\neq}_{mic}/n_m \sim 1\ kT$ (2 kT for Ca^{+2} – CL, because of its dimeric structure). It seems reasonable to assume a figure half as large for IMI formation, which yields

$$G^{\neq}_{mic} \sim (2\pi n_m)^{1/2}\left(\frac{kT}{2}\right). \tag{71}$$

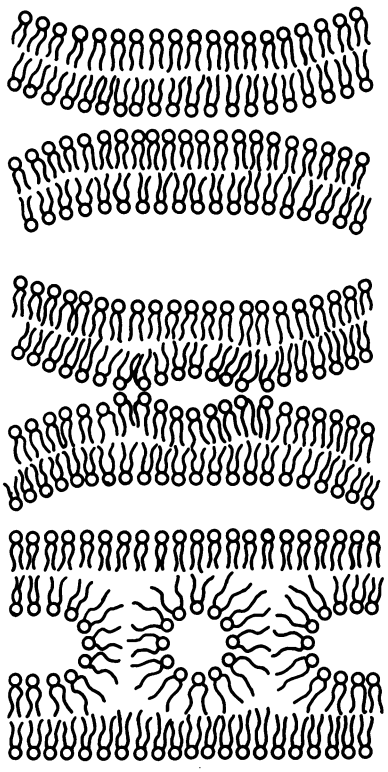

FIGURE 3 Initial events in IMI formation. *Top:* two bilayers are apposed. *Middle:* the lipids at the periphery of a patch containing n_m molecules become closely apposed. Interactions between head-groups at the same interface are disrupted and develop between head groups on opposite interfaces. The radius of curvature of the interfaces begins to decrease. *Bottom:* micelle formation.

IMI Reversion: Membrane Fusion and the $L \rightarrow H_{II}$ Phase Transition. Reversion of IMI to bilayer structure (Fig. 2 *c*) is assumed to proceed via a two-step process. First a concentration fluctuation occurs in the monolayer regions surrounding the inverted micelle. If this fluctuation is large enough to permit re-formation of two apposed membrane interfaces of area A, bilayer formation occurs with a probability F_{-3} by the reverse of the IMI formation process described above. The IMI reversion rate (events/second) P_{-3} is then

$$P_{-3} = f P_c F_{-3}, \tag{72}$$

where P_c is the probability of the critical fluctuation and f is approximately the value given by Eq. 60.

IMI reversion is harder to model than LIP reversion. First, the arrangement of the bilayer attachments to the IMI may change quickly after IMI formation (Fig. 2 *b*). The angles between the planes of the bilayers attached to the periphery of the micelle (viewed in cross section in Fig. 2 *b*) will become equal. This lowers the free energy slightly since it reduces the average interfacial radius of curvature at the bilayer-micelle junctures and distributes strains equally between them. We do not know how quickly or to what extent this happens and thus it is difficult to calculate the local lipid concentrations and the required critical fluctuations for reversion.

Second, the IMI can form two types of bilayer structures (Fig. 2 *c*). It may re-form the original bilayers (bottom right) or form a structure in which the two original lamellae are continuous (left). The latter process is membrane fusion, since a cusplike bilayer annulus joins the original lamellae. The type of final structure formed from an IMI is determined by where the majority of the molecules in a micelle go during the rearrangement. Rearrangement around the vertical axis of symmetry (vertical dashed line in Fig. 2 *b*) produces membrane fusion, and rearrangement about the horizontal plane (horizontal dashed line) re-forms the original bilayers.

It is likely that the critical fluctuations permitting rearrangement of IMI are quite frequent. Fluctuations in any of the three monolayers bounding the micelle (or any combination of them) could permit the rearrangement to start. The alkyl chains of the lipid molecules bordering the micelle are highly disordered, so that local values of C_s will be large. Moreover, we note that no critical fluctuation is required for reversion from the IMI as it is first formed (Fig. 2 *a*): $\tilde{n}_c = 0$ for IMI formation when $r_i = r_0$, and reversion is just the reverse of this process. Therefore, it is reasonable to assume that $P_c = 1$ in Eq. 72.

The two possible bilayer structures probably form with roughly equal frequencies. This seems particularly likely from an IMI geometry like that of Fig. 2 *b*. We will assume that half of the IMI that revert will fuse the original lamellae (Fig. 2 *c*). Using $P_c = 1$ and a form of F_{-3} like

that of F_3 and F_1 (Eq. 16)

$$P_{-3} = \alpha_1 \exp\{-G_-^{\neq}/kT\} \tag{73}$$

and the IMI half-life, $t_{1/2}$, is given by

$$t_{1/2} = (2P_{-3})^{-1}. \tag{74}$$

$G_-^{\neq}$ is the free energy of activation for the reversion process. $G_-^{\neq}$ will not contain a term like $G_{def}^{\neq}$ in $G^{\neq}$ because no new surfaces with unfavorable radii of curvature are formed during reversion. Close to the L $\rightarrow$ H_{II} phase transition of the lipid, we assume that $G_-^{\neq}$ will be approximately equal to $G_{mic}^{\neq}$.

IMI may be intermediates in the L $\leftrightarrow$ H_{II} transitions. Consider lipid bilayers apposed under conditions such that H_{II} is the stable phase at equilibrium. When IMI form under these conditions, they will revert more slowly than when the system is just below the bulk L $\rightarrow$ H_{II} transition. This is because $G_-^{\neq}$ increases. The micellar lipids of the IMI are in conformations resembling those of H_{II} phase lipid more closely than those of lamellar lipid. When the chemical potential difference, $\Delta\mu$, between lamellar and H_{II} phase lipid is positive, a larger $G_-^{\neq}$ will be required to force these lipids back into the lamellar phase. As the H_{II} phase becomes more stable, $G_-^{\neq}$ will increase, P_{-3} decreases, and $t_{1/2}$ increases. That is,

$$G_-^{\neq}]_{\text{above L} \rightarrow H_{II}} \sim G_-^{\neq}]_{\text{at L} \rightarrow H_{II}} + n_m \Delta\mu. \tag{75}$$

$G^{\neq}$ may decrease for similar reasons. Under these conditions, IMI still form rapidly between apposed bilayers, but will endure longer; they will therefore become more numerous. If IMI are consumed by no process other than reversion, the steady state number of IMI per unit area, n_I, will be

$$n_I = \{A[1 + \exp\{(G^{\neq} - G_-^{\neq})/kT\}/P_a]\}^{-1}. \tag{76}$$

As $\Delta\mu$ increases, the more numerous IMI, diffusing in the plane of the apposed bilayers, will encounter other IMI more frequently. Aggregation of IMI into strings will then occur (Fig. 4). The micelles in the string can then rearrange into H_{II} rods within the enveloping monolayer. Aggregation in this manner reduces the free energy of the system. First, the micellar lipid can form the more stable H_{II} rod. Second, aggregation decreases the positive curvature (i.e., head groups splayed apart) of the "waist" of the IMI (the circumference of the semitorroidal surface; Figs. 2 *a*, 4 [top]). As discussed in section A, positive curvature tends to expose hydrophobic moieties to the aqueous phase.

There is morphological evidence of this process. Many workers have published freeze-fracture electron micrographs of spherical features aggregating in strings to form (or blebbing off of) H_{II}-like tubes (5, 8, 20), and many have remarked on the tendency of lipidic particle features to form linear arrays (e.g., 3, 16).

The above model also predicts that thermotropic L $\rightarrow$ H_{II} transitions should be broad and hysteretic. Near T_H, $\Delta\mu \sim \Delta H_H[1 - T/T_H)$, where ΔH_H is the enthalpy of the L $\rightarrow$ H_{II} transition. As noted in section A, these enthalpies are usually small ($\sim$0.5 kT at T_H for EPE [27]), and the $\Delta\mu$ is very small for temperatures close to T_H. Accordingly $(G_-^{\neq} - G^{\neq})$ and thus n_I will change slowly with increasing T (Eq. 76). Since the rate of IMI aggregation must depend on n_I, this implies that the IMI aggregation and reversion rates will be nearly equal over a finite temperature range. For finite heating rates, this produces a broad, hysteretic transition. Such broad, hysteretic thermotropic transitions are observed for EPE and other unsaturated PE (23, 27).

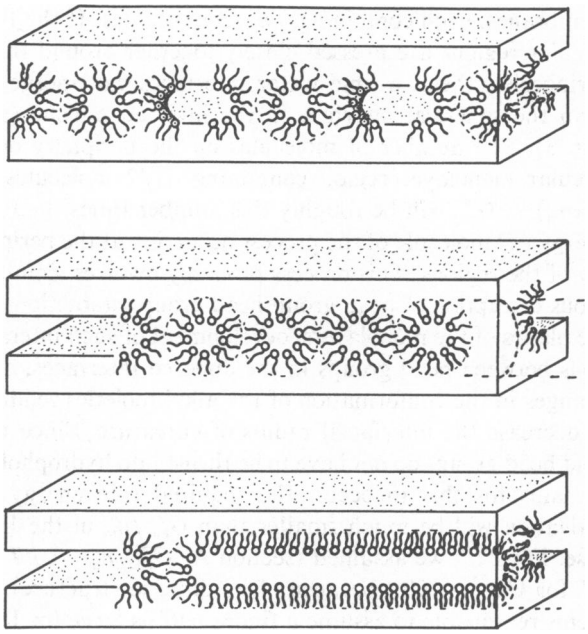

FIGURE 4 IMI aggregation into H_{II} rod precursors. *Top:* many IMI form between apposed lamellae. *Middle:* IMI encounter others and aggregate forming strings of inverted micelles enveloped by the lipid monolayers of the apposed lamellae. *Bottom:* micelles aggregate into elongated cylindrical micelles (H_{II} rod precursors). Only the lipid molecules composing the IMI and the H_{II} rod precursors are depicted.

L $\rightarrow$ H_{II} transitions driven by lipid-divalent cation complex formation (e.g., Ca^{+2}-CL) may be hysteretic under some circumstances. Ca^{+2} binding allows the CL molecules to adopt the small interfacial radii of curvature in the H_{II} phase, so $\Delta\mu$ is probably a sensitive function of the molar ratio of bound Ca^{+2}/CL. This ratio changes rapidly with increasing $[Ca^{+2}]$ (e.g., from 0.35 to 1 for $[Ca^{+2}] \simeq 1$ and 2 mM, respectively; [24]). Thus, $(G^{\neq} - G_-^{\neq})$ and n_I should change rapidly with increasing $[Ca^{+2}]$, indicating a nonhysteretic transition. When CL liposomes are exposed to constant $[Ca^{+2}]$ near the transition threshold concentration, the H_{II} phase does form readily (24).

However, when transiently exposed to $[Ca^{+2}] \gg$ the threshold value $[Ca^{+2}]_t$, many lipidic particles are observed in electron micrographs of the sample (24).

Moreover, ^{31}P-NMR spectra of the samples have intense isotropic resonances that endure for macroscopic intervals. These observations could mean that IMI formed at high [Ca^{+2}] revert and aggregate very slowly. This might be due to a higher bound Ca^{+2}/CL ratio obtained by exposure to high [Ca^{+2}]. Large Ca^{+2}/CL ratios stabilize small interfacial radii of curvature. A ratio close to saturation (Ca^{+2}/CL = 1) might slow the rate at which IMI aggregate and form H_{II} rods. The curvature of the interfaces within the inverted micelle and around the exterior of the IMI must change during this process. At Ca^{+2}/CL ratios near unity, a significant fraction of the Ca^{+2}/CL complexes have to dissociate in order for rearrangement into H_{II} rods to occur. The simultaneous dissociation of many complexes is probably an infrequent event. IMI formed above the $[Ca^{+2}]_t$ probably aggregate slowly, forming strings of inverted micelles packed between lipid monolayers that slowly aggregate into H_{II} rods (Fig. 4, bottom). Moreover, micelles of IMI formed during transient exposure to high [Ca^{+2}] would maintain their high bound Ca^{+2}/CL ratios for long periods, because the lipids surrounding the water cavity of the micelle are almost impermeable to Ca^{+2}. This is consistent with the long-lived isotropic ^{31}P–NMR resonance observed after such transient exposure to [Ca^{+2}] > $[Ca^{+2}]_t$ ("addition samples" in [24]). If this model is correct, one would expect the reverse process (the $H_{II} \rightarrow L$ transition, driven by reducing [Ca^{+2}]) to exhibit pronounced hysteresis for similar reasons (low Ca^{+2} permeability, slow H_{II} rod → IMI aggregate transition). This is in fact observed. When the [Ca^{+2}] is reduced below $[Ca^{+2}]_t$, Ca^{+2}-CL preparations exhibit isotropic ^{31}P-NMR resonances and lipidic particle morphologies for extended periods (24).

This treatment of the $L \rightarrow H_{II}$ transition can be adapted to describe the fusion of apposed unilamellar lipid vesicles via IMI: $[\text{vesicle} + \text{vesicle}]_{\text{aggregated}} \xrightarrow{k_f}$ larger vesicle. The rate constant, k_f, and the outcome of IMI formation will change as a function of the system's proximity of the $L \rightarrow H_{II}$ transition. When the system is just below the $L \rightarrow H_{II}$ transition and reversion is a rapid process, the equation of k_f is a straightforward generalization of Eq. 65

$$k_f = \alpha_1 \left(\frac{A}{A}\right) \exp\{-G^{\neq}/kT\} P_v(1/2) \qquad (77)$$

(valid for $P_v \exp\{(G_-^{\neq} - G^{\neq})/kT\} < 1$). P_v is the probability that the vesicles become closely enough apposed for IMI formation over an area A. The factor of ½ accounts for the fact that only half of IMI reversion events result in fusion (Fig. 2 *c*). The inequality states that this equation applies when IMI formation is rate-limiting (i.e., slower than IMI reversion). In general, this is true just below the $L \rightarrow H_{II}$ transition. Note that under these conditions the walls of the vesicles separating the enclosed volumes from the external aqueous phase do not rupture. IMI reversion makes the walls of the two vesicles continuous, forming a single larger vesicle. The volumes enclosed by the vesicle bilayers become continuous only with each other and not with the external medium. This is obvious from Fig. 3; reversion is just the reverse of the depicted process. Thus, just below the $L \rightarrow H_{II}$ transition, the vesicles fuse without leaking their contents to the external medium.

When the inequality under Eq. 77 is violated, the rate of fusion is limited by the rate at which IMI revert, rather than the rate at which they form (Eq. 77). This will be the case above the $L \rightarrow H_{II}$ transition, when H_{II} is the stable phase at equilibrium and $G_-^{\neq}$ is large

$$k_f = P_{-3}/2 \qquad (78)$$

(for $P_v \exp\{(G_-^{\neq} - G^{\neq})/kT\} > 1$).

Above the transition, however, IMI can aggregate into H_{II} rods between the apposed bilayers (Fig. 4). This process must be rapid compared with IMI reversion above the $L \rightarrow H_{II}$ transition in order for the transition to occur via this model. H_{II} rod formation will progressively transform the vesicle aggregate into a mass of H_{II} lipid. This must eventually lead to release of the encapsulated contents of the original vesicles to the external medium. All the bilayers of the aggregate must be apposed in order to form the H_{II} phase. If so apposed, they cannot separate the original enclosed volumes of the vesicles from the external medium. Therefore, when vesicles are apposed above the $L \rightarrow H_{II}$ transition, the rate at which the IMI aggregate and induce leakage of the apposed vesicles will become significant compared with the rate at which the apposed vesicles fuse.

Rapid IMI aggregation can occur only if a large number of IMI per unit area can form quickly. Therefore, the leakage rate will be small compared with the fusion rate for vesicles apposed over an area A that is less than several multiples of A, and larger for large values of A. Small vesicles may have substantial leakage rates during initial vesicle encounters only if multivesicular aggregates form rapidly on a time scale of k_f^{-1}. Vesicles in the interior of such aggregates could be closely apposed to others over almost their entire surface area, so that $A \gg A$. This will only be true if the vesicle concentration is very high and the long range repulsive forces between vesicles are weak.

We cannot predict the rate of IMI aggregation. However, the lifetime of IMI with respect to aggregation, t_a, will decrease and approach the reversion lifetime $(P_{-3})^{-1}$ at the transition, with $t_a < (P_3)^{-1}$ above the transition. If we define an apparent rate constant k_ℓ for leakage of the contents of aggregated vesicles

$$k_\ell < 1/t_a = P_{-3} \qquad (79)$$

$$(A \gg A).$$

It is apparent that far above the transition, when the inequality under Eq. 78 is satisfied, k_ℓ will become significant compared with k_f. (Because only one IMI need revert to fuse two apposed vesicles, but many must aggregate to

induce leakage, it is likely that $k_f \geqslant k_\ell$ under most circumstances.) In contrast, when the system is nearer the $L \rightarrow H_{II}$ transition, reversion is more rapid than aggregation and k_ℓ is smaller relative to k_f.

Therefore, when vesicles of H_{II}-forming lipid are apposed, the following behavior should be observed. Just below the $L \rightarrow H_{II}$ transition, vesicles should fuse with retention of their contents with a rate constant given by Eq. 77. k_f should increase with increasing proximity to the $L \rightarrow H_{II}$ transition since $G^{\neq}$ decreases. Above the transition, k_f will be given by Eq. 78. The rate of leakage, k_ℓ, from apposed vesicles ($A \gg A$) should be small at the transition, but the ratio of k_ℓ/k_f will increase rapidly farther above the transition. k_{ℓ/k_f} will most likely always be <1. For small vesicles ($A \sim A$), k_f for initial vesicle encounters will be much larger than k_ℓ even far above the transition. Under these circumstances, the vesicles will fuse with retention of contents until they grow large enough for A to become $\gg A$ or multivesicular aggregates form, after which (k_ℓ/k_f) will increase. $G^{\neq}$ and $G^{\neq}_{-}$ change slowly around the $L \rightarrow H_{II}$ transition for thermotropic systems, so that changes in fusion behavior around the transition will be less marked in these systems than in systems with transitions driven by divalent-cation binding.

Predicted Rates for EPE and Ca^{+2}/CL. For EPE (pH 7, $T = T_H$), we assume that $\bar{a}$, a_0, and ℓ have the same values as used in the first part of section A entitled One-Component Systems. Via Eq. 64, we find that $r_0 = 1.67$ nm. This value is close to the radius of the water cavity in the H_{II} phase. It is therefore likely that inverted micelles can form with this value of r_m, and Eq. 65 is the appropriate expression for the IMI formation rate. Using $\alpha_1 = 10^8$ s^{-1}, $T = T_H$, and Eqs. 53, 65, 66, 70, 71, 73, 74, and 77, we obtain $G^{\neq} = 14.0\ kT$, $G^{\neq}_{-} = 11.4\ kT$, and $N_3 \simeq 4.9 \times 10^5$ (P_a) IMI/μm^2/s; $t_{1/2} \simeq 4.5 \times 10^{-4}$ s; $k_f \simeq 42\ (A/A)\ P_v\ s^{-1}$. For small unilamellar vesicles ~ 30 nm in diameter, $A \sim A$ and we can calculate P_v using measurements of interlamellar forces (62, 63). Aggregated EPE vesicles of this size have an equilibrium separation of 1.7 nm and require an activation energy, G_a, of $\sim 10\ kT$ at $T \sim T_H$ (62) to become closely apposed (separation <1 nm). Thus, using

$$P_v \sim \exp\{-G_a/kT\} = \exp\{-10\}, \tag{80}$$

we find $k_f \simeq 0.0019\ s^{-1}$. P_a is the probability of close apposition per interfacial patch of area A in liposomes. P_a is probably $\gtrsim P_v$, so that $N_3 \geqslant 22$ IMI/μm^2/s.

The formation rate of IMI in liposomal dispersions (N_3) is predicted to be more than 10^4 times faster than the LIP formation rate near T_H (section A, One-Component Systems). The predicted half-life near T_H is quite short, however. The predicted rate constant for fusion of aggregated small EPE vesicles is not large, but is sufficient to fuse dispersions in minutes (aggregation is quite rapid for PE vesicles and is not rate limiting [67]). Values for k_f have not been measured for EPE systems. However, in liposomal dispersions of unsaturated PE, fusion (monitored by release of encapsulated marker and electron microscopy) is complete within <5 min (15). This is roughly consistent with the above predictions if we assume $P_a \sim P_v$.

The 0.45 ms half-life estimated for EPE IMI has two consequences concerning experimental observation of IMI. First, the lability of IMI should make them difficult to image via electron microscopy near T_H. IMI form rapidly under such conditions, but revert so quickly that few exist at any instant. In liposomal dispersions, large areas of apposed bilayers can be examined easily and this should not be an insuperable problem. In fact, micrographs of liposomal PE do show structures that could represent IMI (e.g., 3). In unilamellar preparations, however, it is very difficult to examine large areas of apposed vesicle contracts. Even when rapid freezing techniques are applied to halt the reversion process, one would have to examine a very large number of vesicle-vesicle contacts to image a single IMI. With apparatus such as that developed by Heuser (68), for example, a thin layer of sample can be frozen without crystalline artifacts within ~500 μs. If we assume that all IMI formed during this interval are imageable, the number, N, of complete cross fractures of vesicle-vesicle contracts that must be examined to image a single IMI is

$$N \sim (2\ k_f)^{-1}\ (500\ \mu s)^{-1} = 5 \times 10^5. \tag{81}$$

This is quite difficult to do, and may explain why IMI have not been observed in unilamellar PE dispersions (3, 17).

The second consequence of the short half-life is that pure EPE IMI might not produce the "isotropic" ^{31}P-NMR signals expected of micellar structures. Isotropic peaks are observed if some of the lipids experience isotropic motional averaging within intervals shorter than the inverse width of bilayer ^{31}P-NMR peaks (0.1–1 ms). Diffusion of lipids around two surfaces in the IMI can produce such averaging, the semi-torroidal annulus and the spherical interface in the micelle. The former surface contains more than five times more lipid than the latter and has the major effect on the ^{31}P-NMR spectra. For EPE IMI, the two-dimensional random-walk diffusion time, t_m, around this circumference $2\pi(r_m + \ell)$ is

$$t_m \sim \pi^2\ (r_m + \ell)^2/D_s \sim 0.1\ \text{ms}. \tag{82}$$

Note that this is approximately the same as the estimated IMI half-life. Therefore, near T_H IMI may not exist long enough to produce significant isotropic components in the ^{31}P-NMR spectra. (Moreover, the steady state number, n_I, of IMI contain a small fraction of the total EPE in a bilayer dispersion at any given instant, see Eq. 76.) In fact, no such components are observed in spectra of pure EPE or other single-component unsaturated PE dispersions (3, 23, 60). They are observed in spectra of mixtures of unsatu-

rated PE with lipids that only form lamellar phases (3, 10, 25, 26, 69). Lamellar phase impurities probably increase the number of lipid molecules, n_b, in the IMI structure, since they do not readily form interfaces with small radii of curvature. This would increase $G^{\neq}$ and $G_{-}^{\neq}$, and therefore increase $t_{1/2}$. This would increase the intensity of the isotropic component in the ^{31}P-NMR spectra of the mixture, provided n_l was still significant. The model appears consistent with these observations as well.

For Ca^{+2}-CL with $\bar{a}$, a_0, and ℓ values as in the first part of section A entitled One-Component Systems, we find $r_0 = 1.37$ nm via Eq. 64. This is not much larger than the radius of the H_{II} phase water cavity (0.75 nm, [55]). We therefore assume that $r_i = r_0$ and use Eq. 65 for N_3. Since the cardiolipin molecule is essentially two phosphodiacylglyceride molecules joined together, we double the calculated value of n_m in Eq. 71 to estimate $G^{\neq}$, as in the first part of section A. We assume that the $[Ca^{+2}]$ is the threshold value for the $L \rightarrow H_{II}$ transition, $[Ca^{+2}]_t$. At $T = 298°K$, using $\alpha_l = 10^8\ s^{-1}$, we find $G^{\neq} = 12.7\ kT$, $G_{-}^{\neq} = 11.2\ kT$, and $N_3 \simeq 2.3 \times 10^6\ (P_a)\ IMI/\mu m^2/s$; $t_{1/2} \simeq 0.36$ ms and $k_f \simeq 150\ (A/A)P_v\ s^{-1}$.

The interlamellar forces in this system have not been measured, so we cannot accurately guess P_v and P_a. Near $[Ca^{+2}]_t$, the molar ration of bound Ca^{+2} to CL is ~0.35 (24). P_a and P_v will therefore be substantially less than unity, because the negative electrostatic charge on the bilayer interfaces will be substantial. The bound Ca^{+2}/CL ratio increases rapidly with increasing $[Ca^{+2}]$, however, so that P_v, P_a, N_3, and k_f should increase rapidly. At high $[Ca^{+2}]$, P_a and P_v will approach unity. In dispersions of small vesicles, initially fusion will occur with rate constant k_f given by Eq. 78

$$[Ca^{+2}] > [Ca^{+2}]_t\colon k_f \simeq 700\ s^{-1}$$

$$A \sim A.$$

After the first few fusion events, the small vesicles would grow large enough for leakage to become significant. Note that for $[Ca^{+2}] > [Ca^{+2}]_t$, $P_a \rightarrow 1$ and N_3 is predicted to be large enough to completely convert apposed interfaces to arrays of IMI within a millisecond.

There has been an elegant study of the fusion of dispersions of 0.1 μm diameter vesicles of an equimolar mixture of CL and PC in the presence of Ca^{+2} (70). The qualitative behavior of the system in reference 70 is as predicted in the part of section B entitled *IMI Reversion: Membrane Fusion and the L → H_A Phase Transiton.* Fusion with retention of contents is extremely slow until the $[Ca^{+2}]$ concentration surpasses a well-defined $[Ca^{+2}]_t$ (~9 mM), and then increases rapidly. Between Ca^{+2} concentrations of 9 and 9.5 mM, the initial fusion rate increases more than sixfold. The initial rate of leakage of vesicle contents is much slower than the initial fusion rate at $[Ca^{+2}] \sim [Ca^{+2}]_t$, but increases rapidly with $[Ca^{+2}]$ above $[Ca^{+2}]_t$. The ratio of these initial rates is ~0.1 at 10 mM Ca^{+2}, and 0.4 at 15 mM Ca^{+2}. The vesicle diameters are only several times the diameter of an IMI-forming patch of area A (13 nm). The ratio k_ℓ/k_f would be larger if the vesicles were larger. Both the behavior of the initial fusion rate and the initial leakage rates as a function of $[Ca^{+2}]$ are qualitatively as predicted in section B (Theory section, second part) (Eqs. 77–79). The change in fusion rate is also a function of the change in aggregation rate with increasing $[Ca^{+2}]$, and these results are not a straightforward representation of the $[Ca^{+2}]$ dependence of k_f. Nevertheless, it seems unlikely that the change in aggregation rate between 9 and 9.5 mM Ca^{+2} concentration is large enough to account for a sixfold increase in the fusion rate. According to Fig. 2 of reference 70, the change in initial fusion rate between 10 and 10.5 mM Ca^{+2} is about five times the change between 9 and 9.5 mM. Clearly a well-defined $[Ca^{+2}]_t$, and not a simple change in aggregation rate, is involved.

Values of k_f were not obtained in reference 70 by methods used by others (34, 35). It is clear, however, that the value of k_f predicted for pure Ca^{+2}-CL is orders of magnitude larger than the range of values indicated by the data of reference 70. This is as expected, since the rate in pure Ca^{+}-CL should far exceed the rates in a CL-PC mixture. The presence of PC increases n_m and $G^{\neq}$, and may introduce a demixing probability ($P_D \ll 1$) into the expressions for k_f. Moreover, Ca^{+2}-induced phase separation of CL and PC regions may be necessary before IMI can form rapidly. This would slow the initial fusion rate. The maximum initial rate of fusion observed in reference 70 was fusion of ~30% of the original vesicles in 1s ($[Ca^{+2}]$ = 20 mM, > $[Ca^{+2}]_t$). This is compatible with $k_f > 0.3\ s^{-1}$. The value of k_f predicted for pure Ca^{+2}-CL above $[Ca^{+2}]_t$ is $700\ s^{-1}$.

Note that the value of $[Ca^{+2}]_t$ is sensitive to the proportion of (charged) CL in the lipid mixture and the ionic strength of the suspending medium. This is a simple consequence of the effect of the electrostatic surface potential of the bilayers on the $[Ca^{+2}]$ in the electrical double layer and therefore available for complexation with CL. This effect has been extensively treated in other systems (e.g., 71). For instance $[Ca^{+2}]_t$ is ~ 9 mM in equimolar CL-PC mixtures (70) and is only ~1 mM for pure CL in a similar medium (24).

As noted in the part of section B entitled *IMI Reversion: Membrane Fusion and the L → H_{II} Phase Transition,* our model of IMI formation and aggregation is qualitatively compatible with the behavior of Ca^{+2}/CL systems underdoing the $L \rightarrow H_{II}$ transitions (24). Near $[Ca^{+2}]_t$, the enormous value of N_3 we predict (sufficient to completely convert apposed bilayers to IMI arrays in milliseconds) is compatible with a facile $L \rightarrow H_{II}$ transition. The predicted value of $t_{1/2}$ is short enough to explain the very weak isotropic ^{31}P-NMR resonances observed under these circumstances. Not only do IMI disappear rapidly due to IMI aggregation, but they revert so quickly that the average

lifetime is approximately the NMR time scale (0.1–1 ms). Because IMI also represent a small fraction of the total lipid population at any instant, they have a minimal effect on the ^{31}P-NMR spectrum of the mixture, as observed. We postulate that IMI aggregation into (and disaggregation from) H_{II} rods is slower at $[Ca^{+2}] > [Ca^{+2}]_t$. Careful rapid-freezing freeze-fracture studies will be necessary to prove this.

The rates and half-lives predicted above for EPE and Ca^{+2}-CL are only estimates. The values are sensitive to the values we estimate for $G^{\neq}$, $G^{\neq}_{-}$, and α_1. For example, the largest contribution to $G^{\neq}$ and $G^{\neq}_{-}$ is $G^{\neq}_{mic}$, which we can only crudely estimate. An error of 4 or 5 kT in our estimate of $G^{\neq}_{mic}$ would change N_3, k_f, and $t_{1/2}$ by two orders of magnitude. The chief result of these calculations is that the predicted values of N_3, k_f and $t_{1/2}$ are consistent with the observed behavior of EPE and Ca^{+2}-CL systems for reasonable estimates of the input parameters.

At present, there is no direct evidence for the existence of IMI structures. ^{31}P-NMR and some morphological results are consistent with our model of such structures, however. Higher-resolution rapid-freezing morphological studies of lipidic particle images in systems undergoing the $L \rightarrow H_{II}$ transitions might provide more direct evidence for the type of structure envisioned here. For systems like Ca^{+2}-CL, this work might best be conducted on samples transiently exposed to $[Ca^{+2}]$ significantly greater than $[Ca^{+2}]_t$; under such circumstances, the half-lives of IMI are probably longer than at $[Ca^{+2}]_t$.

It would be surprising if structures resembling IMI did not exist. The inverted geometry of the H_{II} phase cannot arise quickly from intrabilayer events such as LIP formation (e.g., LIP formation followed by LIP aggregation into H_{II} rods enveloped by the leaflets of the original bilayer). Even the maximum LIP formation rates calculated in section A are too slow to account for $L \rightarrow H_{II}$ transitions that occur in minutes or less. Ca^{+2}-CL LIP form at less than ~250 LIP/μm^2/h; this means that <2% of the lipid would be converted to H_{II}-like geometry per hour at $[Ca^{+2}]_t$. It is difficult to imagine another intrabilayer event that could give rise to the H_{II} phase and yet proceed at an appreciable ra One might imagine lengths of cylindrical inverted micelle forming in a manner analogous to LIP, for instance, but this process would involve the simultaneous translocation of many more molecules across the monolayers than in the LIP case; the activation energy would be prohibitive and the rate trivial. The inverted geometry of the H_{II} phase must therefore involve an interbilayer event, which seems to require the existence of structures like IMI.

IMI might be intermediates in the process of unilamellar vesicle fusion. In this case, however, other processes leading to membrane fusion (but not H_{II} phase formation) may occur at competitive rates. Membrane fusion in unilamellar dispersions of phosphatidylserine (PS) in the presence of Ca^{+2} obviously proceeds via a different mechanism, because PS has never been observed to adopt the H_{II} phase in the presence of Ca^{+2}. Fusion in this system has been extensively studied (29–33). The critical defect responsible for bilayer fusion by this mechanism is thought to be the periphery of the gelled, divalent cation-complexed lipid patches formed between the closely-apposed membranes (29, 33, 75). This mechanism is probably relevant to other acidic phospholipid systems as well. The fusion rate constants for this mechanism are clearly competitive with the rate constants we estimate here for IMI-mediated fusion. Nir et al. (34, 35) have measured k_f values for small PS vesicles of $5 \pm 3\ s^{-1}$. This is probably comparable with k_f for CL at $[Ca^{+2}]_t$, $k_f \simeq 150\ (P_v)$, where $P_v < 1$. However, it is less than k_f for CL at $[Ca^{+2}] > [Ca^{+2}]_t$. By comparison, the predicted IMI-mediated k_f for small EPE vesicles is only $\sim 0.002\ s^{-1}$. For mixed systems of H_{II}-forming lipids and acidic phospholipids (e.g., EPE/PS), or for systems where divalent cation binding drives the $L \rightarrow H_{II}$ transition (e.g., Ca^{+2}-CL), it might be difficult to determine whether the initial vesicle fusion events take place via IMI-mediated or Ca^{+2}-PS-like mechanisms. Careful measurements of k_f as a function of temperature near T_H or divalent cation concentration might aid in making this distinction.

Several investigators have reported results they interpret as excluding involvement of lipidic particles as fusion intermediates. It is important to distinguish between LIP and IMI in this matter. Bearer et al. (19) conducted an interesting rapid-freezing electron microscopic study of vesicles of equimolar CL/PC mixtures and equimolar EPE/brain PS mixtures. These vesicles were incubated with 5 mM Ca^{+2} for 1–2 s before rapid freezing. The authors reported no lipidic particles structures visible on the vesicles, although fusion occurred. They concluded that lipidic particles, which only occurred in their dispersions after hours of incubation, were not involved in fusion.

While this type of study may eventually tell us much about inverted micellar structures, work so far does not rule out an IMI fusion mechanism. First, as the authors of reference 19 pointed out, their work does not exclude the possibility of a transitory IMI-like intermediate. Here, we predict IMI to have submillisecond half-lifes. Such intermediates would be very difficult to image in unilamellar dispersions via this technique (Eq. 81) and would probably escape detection. The lipidic particle images visible after prolonged incubation probably represent LIP, which we predict to form at rates compatible with the observations of reference 19. These structures are long-lived and should be more easily detected. LIP are intrabilayer structures, uninvolved in membrane fusion (section A). Second, the CL/PC vesicles in reference 19 were incubated under conditions in which IMI are unlikely to form: 5 mM Ca^{+2} in the presence of 100 mM NaCl at pH 7.4. In a more recent study using nearly identical media, Wilschut et al. (70) found that $[Ca^{+2}]_t$ is ~9 mM for the same lipid mixture. Thus it would be even more difficult to detect the

formation of IMI structures in such dispersions, since IMI might not form at all. Wilschut et al. (70) could barely measure fusion rates even at 8 mM Ca^{+2}. Under these circumstances ($[Ca^{+2}] < [Ca^{+2}]_t$) it would not be surprising if another mechanism (resembling the Ca^{+2}-PS mechanism) was responsible for fusion. In contrast, at higher $[Ca^{+2}]$ the sharp threshold $[Ca^{+2}]$ and extraordinarily rapid increase in fusion rate with increasing $[Ca^{+2}]$ (70) seem more consistent with an IMI fusion mechanism (see the preceding part of this section). The absence of lipidic particles in PE-brain PS dispersions after short incubations (19) reflects the disparity between the rate of fusion in the Ca^{+2}-PS system and the predicted (IMI-mediated) rate in PE (below).

There have been several excellent investigations of the fusion process in mixtures of unsaturated alkyl-chain PE and PS (73, 74). In these studies, divalent cation-induced fusion, presumably involving PS, dominated the initial fusion rate. In reference 73, fusion occurred rapidly even though the temperature was said to be below T_H for the PE component. In reference 74, transbilayer redistribution of PE (indicating the presence of nonbilayer PE structures, like IMI [75]) occurred only after extensive Ca^{+2}-induced fusion, presumably via fusion of regions of nearly pure PS that laterally phase separate upon addition of Ca^{+2} (74, 76, 77). However, these observations are in accord with the present model of IMI formation. k_f for Ca^{+2}-induced small PS vesicle fusion is much larger than the predicted k_f for small EPE vesicles. Thus, membrane fusion of patches of PS on apposed interfaces should be much faster than fusion of PE via IMI, as is observed in both studies (73, 74). Naturally, if the system is far below T_H, IMI cannot form and fusion proceeds via a different mechanism. As noted in reference 74, nonbilayer PE structures form when equimolar PE/PS is incubated with Ca^{+2} but not with Mg^{+2}. This is because Mg^{+2} does not induce extensive PS phase separation, whereas Ca^{+2} is much more effective (76). The rate of IMI formation in incompletely phase-separated PE/PS mixtures will be quite small. The non-H_{II}-forming PS will increase n_m and $G^{\neq}$, as well as introduce a P_D term ($\ll 1$) into the expressions for k_f and N_3 (Eqs. 61, 63, 65, 77).

The rate of IMI formation in EPE is also dependent on the rate at which the membranes can be closely apposed. In mixed PE-PS membranes, Mg^{+2} or Ca^{+2} binding will closely appose the interfaces (via charge neutralization and "dehydrated" complex formation in the case of Ca^{+2} [79]). Thus, the rate of nonbilayer structure (IMI) formation in liposomes will be effected by the accessibility of inner lamellae of liposomes to Ca^{+2}. Ca^{+2} is necessary to closely appose and laterally phase separate the lamellae. This may explain the vesicle radius of curvature effect found in reference 74. Transbilayer PE redistribution was found only in situations when small unilamellar PE-PS vesicles (SUV) were added with PE-PS liposomes to Ca^{+2}-containing media above T_H. k_f for SUV (at least for pure PS SUV) is much larger than for larger vesicles (5 ± 3 vs. $0.1\ s^{-1}$ [34, 35]). If true for PE-PS structures as well, small vesicles would fuse more rapidly with each other (Ca^{+2}-PS mechanism) than with liposomes. (Repulsive forces between particles are also smaller for small structures.) After the first few fusion events, fusing PS SUV dispersions become leaky (78, 79). These structures would now contain Ca^{+2}. Fusion of these larger structures with the original liposomes would introduce Ca^{+2} into the liposomal interlamellar spaces, driving close apposition, PS-PE phase separation, and IMI formation. This would produce the observed (74) transbilayer PE redistribution.

Sundler et al. (80) also concluded that nonbilayer phase formation is not involved in fusion of phosphatidylinositol (PI)-PE mixtures in the presence of Ca^{+2} and Mg^{+2}. Above the gel $\rightarrow$ liquid crystalline transition temperature of the lipids, vesicles of such mixtures fuse at comparable rates whether or not the PE component is EPE or dimyristoyl PE (which does not form the H_{II} phase under these conditions [81]). Vesicles of pure PI do not fuse (80). One might infer that PE is itself the lipid component undergoing the fusion process and that no IMI is involved because of the effectiveness of dimyristoyl PE. However, this could just as well represent a fusion mechanism involving predominantly PI which is faster than the sluggish IMI fusion rate predicted for EPE. It is noted in reference 80 that increasing proportions of PE decrease the $[Ca^{+2}]$ and $[Mg^{+2}]$ necessary to induce fusion of PE-PI vesicles. The role of PE may be to simply facilitate close apposition. PE head groups are comparatively poorly hydrated, and the short-range repulsive "hydration" forces between PE lamellae are weak compared with other lipids (62), as noted in reference 80. Increasing the ratio of neutral PE to charged PI thus reduces both the head group hydration of and electrostatic repulsive forces between the vesicles. This will increase the frequency of close apposition, which is a prerequisite to fusion via either mechanism. Pure PI vesicles may simply become closely apposed so infrequently due to their high surface charge and well-hydrated head groups as to fuse at negligible rates. It is also interesting to note that soy PE-soy PI mixtures have recently been reported to form lipidic particles in the presence of Ca^{+2} (82). Therefore, an IMI fusion mechanism is possible in this system with a PE component above T_H. As in the PE-PS case, these findings (80) do not rule out an IMI fusion mechanism. They do demonstrate that the rate of such a mechanism, if it exists, must be slower than the rate observed for the Ca^{+2}-induced (non-IMI) mechanism. Given the slow rate predicted here for EPE, this is not surprising. In contrast, the predicted IMI fusion rate for the Ca^{+2}-CL system is very rapid. The sharp $[Ca^{+2}]_t$ and extraordinarily rapid increase in fusion rate for $[Ca^{+2}] > [Ca^{+2}]_t$ observed for the CL/PC system, as well as the rapidity of the lamellar $\rightarrow$ H_{II} transition at $[Ca^{+2}]_t$ (24), are good indications that Ca^{+2}-CL fusion does proceed via an IMI mechanism.

Conclusions Concerning IMI

The estimated rates and half-lives of IMI indicate that these structures should have the following properties. First, they should form quite readily between apposed membranes, at rates several orders of magnitude faster than LIP formation in isolated membranes. This could explain the rarity of lipidic particle images in unilamellar preparations of lipids that form many such particles in liposomal preparations under the same conditions. In liposomes, the fraction of apposed membrane surface area is quite large, and IMI should form frequently, giving rise to lipidic particle morphology. In unilamellar vesicle dispersions, the fraction of apposed area is much smaller, and IMI should be less frequent. Any lipidic particle structures observed in these cases probably represent LIP (which form much less frequently, see section A or IMI formed at planes of vesicle-vesicle contact. This idea has been previously proposed (e.g., 2, 3, 5, 12–14).

Second, IMI half-lives are predicted to be quite short. These half-lives are comparable with the ^{31}P-NMR time scale in pure lipid preparations close to the L $\rightarrow$ H_{II} transition. This (and the small fraction of lipid present as IMI at any instant) is compatible with the absence or near absence of "isotropic" ^{31}P-NMR resonances under these conditions (2, 23, 24, 60) and the greater intensity of such resonances when IMI reversion and aggregation rates are predicted to be slower (e.g., incorporation of lamellar phase impurity; [10], [25], [60]; see also the section entitled *IMI Reversion: Membrane Fusion and the L $\rightarrow$ H_{II} Phase Transition*). These short half-lives also indicate the difficulty in imaging IMI in fast-freezing experiments (Eq. 81).

Third, the fusion rates constants predicted for EPE and Ca^{+2}-CL are compatible with observation (see the final part of the Theory section in section B). The rate constant predicted for EPE is small compared with rate constants for the Ca^{+2}-PS fusion mechanism (30–32), indicating that in mixed lipid systems the fusion rate may be dominated by other mechanisms. The rate constant for Ca^{+2}-CL is quite large, however, which is compatible with the very rapid fusion observed in the similar Ca^{+2}-CL/PC system (70). Our model is also consistent with the qualitative behavior of k_f and the relative significance of vesicle-vesicle leakage vs. fusion as a function of [Ca^{+2}] in this system. It is emphasized that the IMI fusion mechanism is not proposed as an alternative explanation for fusion in systems like PS in the presence of Ca^{+2}. IMI fusion can only occur in lipid systems with components near their lamellar-to-H_{II} phase transitions. As far as we know, pure PS does not adopt such a phase with or without Ca^{+2} under normal conditions. IMI fusion is a likely candidate in other systems. This work provides a means of estimating the rate via this mechanism in comparison with alternative processes. Fusion via IMI remains to be demonstrated. Higher-resolution rapid freezing morphological investigations seem necessary to do this. Fourth, this model of IMI formation is compatible with the observed hysteresis in the L $\leftrightarrow$ H_{II} transitions of EPE and Ca^{+2}-CL.

The rates and half-lives calculated in this work are only estimates; the values are very sensitive to the value of $G^{\neq}$ and $G^{\neq}_{mic}$, which cannot be directly measured. The principal result is that reasonable estimates of these parameters based on equilibrium properties yield rates and half-lives consistent with the NMR, morphological, membrane fusion, and L $\leftrightarrow$ H_{II} transition behavior of the relevant systems.

Bilayer systems with the following attitudes will form IMI most readily.

(*a*) Values of $\bar{a}$, a_0, ℓ such that r_0 as calculated by Eq. 64 is within a few tenths of a nanometer of r_i, the radius of the water channel in the H_{II} phase (i.e., $\tilde{n}_c \rightarrow 0$). If this condition is not met, then IMI formation will be fastest when $|n_c|$ given by Eq. 57 is $\ll 1$ and C_s is large.

(*b*) Small $G^{\neq}$, which requires that either $T \geq T_H$ (thermotropic L $\rightarrow$ H_{II} transitions) or [cation] $\geq$ [cation]$_t$ (cation binding-driven transitions).

(*c*) High probability of close apposition of bilayers (i.e., fast aggregation rates and weak short-range repulsive forces between interfaces).

(*d*) In mixed systems, a large mole fraction of H_{II}-forming component. Small mole fractions will still be effective if the lipid mixing is nonideal or phase separation of the H_{II}-forming component can be achieved by other means. Examples are cation binding to acidic lipid components (e.g., 76) or separation induced by close apposition itself (63).

The author is grateful to D. F. Hager for many valuable discussions.

Received for publication 28 October 1982 and in final form 27 June 1983.

REFERENCES

1. Verkleij, A. J., C. Mombers, J. Leunissen-Bijvelt, and P. J. J. Th. Ververgarert. 1979. Lipidic intramembranous particles. *Nature (Lond.)* 279:162–163.
2. Sen, A., W. P. Williams, A. P. R. Brain, and P. J. Quinn. 1982. Bilayer and non-bilayer transformations in aqueous dispersions of mixed sn-3-galactosyldiacylglycerols isolated from chloroplasts. *Biochim. Biophys. Acta.* 685:297–306.
3. Hui, S. W., T. P. Stewart, P. L. Yeagle, and A. D. Albert. 1981. Bilayer to non-bilayer transition in mixtures of phosphatidylethanolamine and phosphatidylcholine: implications for membrane properties. *Arch. Biochem. Biophys.* 207:227–240.
4. Verkleij, A. J., R. DeMaagd, J. Lennissen-Bijvelt, and B. Dekruijff. 1982. Divalent cations and chloropromazine can induce non-bilayer structures in phosphatidic acid-containing model membranes. *Biochim. Biophys. Acta.* 684:255–262.
5. Verkleij, A. J., C. J. A. VanEchteld, W. J. Gerritsen, P. R. Cullis, and B. DeKruijff. 1980. The lipidic particle as an intermediate structure in membrane fusion processes and bilayer to hexagonal H_{II} transitions. *Biochim. Biophys. Acta.* 600:620–624.
6. DeKruijff, B., A. J. Verkleij, C. J. A. VanEchteld, W. J. Gerritsen, C. Mombers, P. C. Noordam, and J. DeGier. 1979. The occurrence of

lipidic particles in lipid bilayers as seen by ^{31}P-NMR and freeze-fracture electron microscopy. *Biochim. Biophys. Acta.* 555:200–209.

7. Sen, A., A. P. R. Brain, P. J. Quinn, and W. P. Williams. 1982. Formation of inverted lipid micelles in aqueous dispersions of mixed sn-3-galactosyldiacylglycerols induced by heat and ethylene glycol. *Biochim. Biophys. Acta.* 686:215–224.
8. VanVenetie, and A. J. Verkleij. 1981. Analysis of the hexagonal II phase and relations of lipidic particles and the lamellar phase. A freeze-fracture study. *Biochim. Biophys. Acta.* 645:262–269.
9. Cullis, P. R., and B. DeKruijff. 1979. Lipid polymorphism and the functional roles of lipids in biological membranes. *Biochim. Biophys. Acta.* 559:399–420.
10. Cullis, P. R., and B. DeKruijff. 1978. Polymorphic phase behavior of lipid mixtures as detected by ^{31}P-NMR. Evidence that cholesterol may destabilize bilayer structure in membrane systems containing phosphatidylethanolamine. *Biochim. Biophys. Acta.* 507:207–218.
11. Burnell, E. E., P. R. Cullis, and B. DeKruijff. 1980. Effects of tumbling and lateral diffusion of PC model membrane ^{31}P-NMR lineshapes. *Biochim. Biophys. Acta.* 603:63–69.
12. Rand, R. P., T. S. Reese, and R. G. Miller. 1981. Phospholipid bilayer deformations associated with interbilayer contact and fusion. *Nature (Lond.).* 293:237–238.
13. Cullis, P. R. and M. J. Hope. 1978. Effects of fusogenic agents on membrane structure of erythrocyte ghosts and the mechanism of membrane fusion. *Nature (Lond.).* 271:672–674.
14. Hope, M. J., and P. R. Cullis. 1981. The role of nonbilayer lipid structures in the fusion of human erythrocytes induced by lipid fusogens. *Biochim. Biophys. Acta.* 640:82–90.
15. Noordam, P. E., C. J. A. VanEchteld, B. DeKruijff, A. J. Verkleij and J. DeGier. 1980. Barrier characteristics of membrane model systems containing unsaturated phosphotidylethanolamines. *Chem. Phys. Lipids.* 27:221–232.
16. Miller, G. G. 1980. Do 'lipidic particles' represent intermembrane attachment sites? *Nature (Lond.).* 287:166–617.
17. Hui, S. W., and T. P. Steward. 1981. 'Lipidic particles' are intermembrane attached sites. *Nature (Lond.).* 290:427–428. See also reply by A. J. Verkleij and B. de Kruijff, ibid., pp. 427–428.
18. Mandersloot, J. G., W. J. Gerritsen, J. Leunissen-Bijvelt, C. J. A. Van Echteld, P. C. Noordam, and J. DeGeir. 1981. Ca^{+2}-induced change in the barrier properties of cardiolipin/phosphatidylcholine bilayers. *Biochim. Biophys. Acta.* 640:106–113.
19. Bearer, E. L., N. Duzgunes, D. S. Friend, and D. Papahadjopoulos. 1982. Fusion of phospholipid vesicles arrested by quick-freezing: the question of lipidic particles as intermediates in membrane fusion. *Biochim. Biophys. Acta.* 693:93–98.
20. Gounaris, K., A. Sen, A. P. R. Brain, P. J. Quinn, and W. P. Williams. 1983. The formation of non-bilayer structures in total lipid extracts of chloroplast membranes. *Biochim. Biophys. Acta.* 728:129–139.
21. Hui, S. W., and L. T. Boni. 1982. Lipidic particles and cubic phase lipids. *Nature (Lond.).* 296:175. (See also reply by W. P. Williams et al. ibid., pp. 175–176.)
22. Cullis, P. R., and B. deKruijff. 1976. ^{31}P-NMR studies of unsonicated aqueous dispersions of neutral and acidic phospholipids. Effects of phase transitions, pH, and divalent cations on motion in the phosphate region of the polar headgroups. *Biochim. Biophys. Acta.* 436:523–540.
23. Cullis, P. R., and B. DeKruijff. 1978. The polymorphic phase behavior of phosphatidylethanolamines of natural and synthetic origin. *Biochim. Biophys. Acta.* 513:31–42.
24. DeKruijff, B., A. J. Verkleij, J. Leunissen-Bijvelt, C. J. A. Van Echteld, J. Hille, and H. Rijnbout. 1982. Further aspects of the Ca^{+2}-dependent polymorphism of bovine heart cardiolipin. *Biochim. Biophys. Acta.* 693:1–12.
25. Cullis, P. R., P. W. M. Van Dijck, B. DeKruijff, and J. DeGier. 1978. Effects of cholesterol on the properties of equimolar mixtures of synthetic phosphatidylcholine and phosphatidylethanolamine: a ^{31}P-NMR and DSC study. *Biochim. Biophys. Acta.* 513:21–30.
26. Tilcock, C. P. S., M. B. Bally, S. B. Farren, and P. R. Cullis. 1982. Influence of cholesterol on the structural preferences of dioleoyl PE-dioleoyl PC systems: a ^{31}P- and ^{2}H-NMR study. *Biochemistry.* 21:4596–4601.
27. Hardman, P. D. 1982. Spin-label characterization of the lamellar-to-hexagonal (H_{II}) phase transition in egg phosphatidylethanolamine aqueous dispersions. *Eur. J. Biochem.* 124:95–101.
28. Verkleij, A. J., C. Mombers, W. J. Gerritsen, L. Leunissen-Bijvelt, and P. R. Cullis. 1979. Fusion of phospholipid vesicles in association with the appearance of lipidic particles as visualized by freeze-fracturing. *Biochim. Biophys. Acta.* 555:358–361.
29. Portis, A., C. Newton, W. Pangborn, and D. Papahadjopoulos. 1979. Studies on the mechanism of membrane fusion: evidence for an intermembrane Ca^{+2}-phospholipid complex, synergism with Mg^{+2}, and inhibition by spectrin. *Biochemistry.* 18:780–790.
30. Nir, S., J. Wilschut, and J. Bentz. 1982. The rate of fusion of phospholipid vesicles and the role of bilayer curvature. *Biochim. Biophys. Acta.* 688:275–278.
31. Nir, S., J. Bentz, J. Wilshut, and N. Duzgunes. 1983. Aggregation and fusion of phospholipid vesicles. *Prog. Surf. Sci.* 13:1–124.
32. Nir, S., J. Bentz, and A. R. Portis, Jr. 1980. Effect of cation concentrations and temperature on the rates of aggregation of acidic phospholipid vesicles: application to fusion. *Adv. Chem. Ser.* 188:75–106.
33. Papahadjopoulos, P., W. J. Vail, C. Newton, S. Nir, K. Jacobson, G. Poste, and R. Lazo. 1977. Studies on membrane fusion. III. The role of Ca^{+2}-induced phase changes. *Biochim. Biophys. Acta.* 465:579–598.
34. Nir, S., J. Wilschut, and J. Bentz. 1982. The rate of fusion of phospholipid vesicles and the role of bilayer curvature. *Biochim. Biophys. Acta.* 688:275–278.
35. Bentz, J., S. Nir, and J. Wilschut. 1983. Mass action kinetics of vesicle aggregation and fusion. *Colloids Surf.* 6:333–336.
36. Sillerud, L. O., and R. E. Barnett. 1982. Lack of transbilayer coupling in phase transitions of phosphatidylcholine. *Biochemistry* 21:1756–1760.
37. Schmidt, C. F., Y. Barenholz, C. Huang, and T. E. Thompson. 1978. Bilayer coupling in sphingomelin bilayer systems. *Nature (Lond.)* 271:775–777.
38. Eigenberg, K. E., and S. I. Chan. The effect of surface curvature on the head-group structure and phase transition properties of phospholipid bilayer vesicles. *Biochim. Biophys. Acta.* 599:330–335.
39. Lawaczeck, R., M. Kainosho, and S. I. Chan. 1976. The formation and annealing of structural defects in lipid bilayer vesicles. *Biochim. Biophys. Acta.* 443:313–330.
40. Blank, M. 1962. Monolayer permeability and the properties of natural membranes. *J. Phys. Chem.* 66:1911–1918.
41. Lis, L. J., M. McAlister, N. Fuller, R. P. Rand, and V. A. Parsegian. 1982. Measurements of the lateral compressibility of several phospholipid bilayers. *Biophys. J.* 37:667–672.
42. Pace, R. J., and S. I. Chan. 1982. Molecular motions in lipid bilayers. III. Lateral and transverse diffusion in bilayers. *J. Chem. Phys.* 76: 4241–4247.
43. Galla, H-J., W. Hartmann, U. Theilen, and E. Sackmann. 1979. On the two-dimensional passive random walk in lipid bilayers and fluid pathways in biomembranes. *J. Membr. Biol.* 48:215–236.
44. Evans, E. A., and R. Waugh. 1977. Mechano-chemistry of closed, vesicular membrane systems. *J. Colloid Interface Sci.* 60:286–298.
45. Cook, G. M. W., W. R. Redwood, A. R. Taylor, and D. A. Haydon. 1968. The molecular composition of black hydrocarbon films in aqueous solutions. *Kolloid Z. Z. Polym.* 277:28–37.

46. Wolfe, J., and P. L. Steponkus. 1981. The stress-strain relation of the plasma membrane of isolated plant protoplasts. *Biochim. Biophys. Acta.* 643:663–668.
47. Villalonga, F. A., R. J. Koftan, and J. P. O'Connell. 1982. Interfacial tensions and partition coefficients in water and N-heptane systems containing n-alkanols, alkylketones, alkylamides, and alkylmonocarboxylic acids. *J. Colloid Interface Sci.* 90:539–549.
48. Reiss-Husson, F. 1967. Structure des phases liquide-crystallines de differents phospholipides, monoglycerides, sphingolipides, anhydres ou en presence d'eau. *J. Mol. Biol.* 25:363–382.
49. Junger, E., and H. Reinauer. 1969. Liquid crystalline phases of hydrated phosphatidylethanolamine. *Biochim. Biophys. Acta.* 183:304–308.
50. Tinker, D. O., and L. Pinteric. 1971. On the identification of lamellar and hexagonal phases in negatively-stained phospholipid-water systems. *Biochemistry.* 10:860–865.
51. Rubenstein, J. L. R., B. A. Smith, and H. M. McConnell. 1979. Lateral diffusion in binary mixtures of cholesterol and phosphatidylcholines. *Proc. Natl. Acad. Sci. (USA).* 76:15–18.
52. Edidin, M. 1974. Rotational and translational diffusion in membranes. *Annu. Rev. Biophys. Bioeng.* 3:179–201.
53. Kwok, R, and E. Evans. 1981. Thermoelasticity of large lecithin bilayer vesicles. *Biophys. J.* 35:637–652.
54. Evans, E., and R. Kwok. Mechanical calorimetry of large dimyristoylphosphatidylcholine vesicles in the phase transition region. *Biochemistry.* 21:4874–4879.
55. Rand, R. P., and S. Sengupta. 1972. Cardiolipin forms hexagonal structures with divalent cations. *Biochemistry.* 255:484-492.
56. Shah, D. O., and J. H. Schulman. 1965. Binding of metal ions to monolayers of lecithins, plasmalogens, cardiolipin, and dicetyl phosphate. *J. Lipid Res.* 6:341–349.
57. Ries, H. E. 1979. Monolayers of mitochondrial and bacterial cardiolipin. *J. Colloid Interface Sci.* 71:625–627.
58. Ries, H. E., and H. Swift. 1982. Monolayers of mitochondrial cardiolipin and cerebronic acid and their equimolar mixtures. *J. Colloid Interface Sci.* 89:245–256.
59. Vasilenko, I., B. DeKruijff, and A. J. Verkleij. 1982. The synthesis and use of thionphospholipids in ^{31}P-NMR studies of lipid polymorphism. *Biochim. Biophys. Acta.* 685:144–152.
60. Tilcock, C. P. S., and P. R. Cullis. The polymorphic phase behavior and miscibility properties of synthetic phosphatidylethanolamines. *Biochim. Biophys. Acta.* 684:212–218.
61. Cullis, P. R., B. DeKriujff, M. J. Hope, R. Nayar, and S. L. Schmid. 1980. Phospholipids and membrane transport. *Can. J. Biochem.* 58:1091–1100.
62. Lis, L. J., M. McAlister, N. Fuller, R. P. Rand, and V. A. Parsegian. 1982. Interactions between neutral phospholipid bilayer membranes. *Biophys. J.* 37:657–665.
63. Rand, R. P. 1981. Interacting phospholipid bilayers: measured forces and induced structural changes. *Annu. Rev. Biophys. Bioeng.* 10:277–314.
64. Cowley, A. C., N. L. Fuller, R. P. Rand, and V. A. Parsegian. 1978. Measurement of repulsive forces between charged phospholipid bilayers. *Biochemistry.* 17:3163–3168.
65. Brouillette, C. G., J. P. Segrest, T. C. Ng, and J. L. Jones. 1982. Minimal size phosphatidylcholine vesicles: effects of radius of curvature on head group packing and conformation. *Biochemistry.* 21:4569–4575.
65a. Cornell, B. A., G. C. Fletcher, J. Middlehurst, and F. Separovic. 1982. The lower limit to the size of small sonicated phospholipid vesicles. *Biochim. Biophys. Acta.* 690:15–19.
66. Saffman, P. G. 1976. Brownian motion in thin sheets of viscous fluid. *J. Fluid Mech.* 73:593–602.
67. Kolber, M. A., and D. H. Haynes. 1979. Evidence for a role of phosphatidylethanolamine as a modulator of membrane-membrane contact. *J. Membr. Biol.* 48:95–114.
68. Heuser, J. E. 1977. Synaptic vesicle exocytosis revealed in quick-frozen frog neuromuscular junctions treated with 4-amino pyridine and given a single electrical shock. *Soc. Neuroci. Symp.* 2:215–239.
69. Farren, S. B., and P. R. Cullis. 1980. Polymorphism of phosphatidylglycerol phosphatidylethanolamine model membrane systems: A ^{31}P-NMR study. *Biochem. Biophys. Re. Commun.* 97:182–191.
70. Wilchut, J., M. Holsappel, and R. Jansen. 1982. Ca^{+2}-induced fusion of cardiolipin/phosphatidylcholine vesicles monitored via mixing of aqueous contents. *Biochim. Biophys. Acta.* 690:297–301.
71. Nir, S., C. Newton, and D. Papahadjopoulos. 1978. Binding of cations to phosphatidylserine vesicles. *Bioelectrochem. Bioenerg.* 5:116–133.
72. Wilschut, J., N. Duzgunes, and D. Papahadjopoulos. 1981. Ca^{+2}/Mg^{+2} specificity in membrane fusion: kinetics of aggregation and fusion of phosphatidylserine vesicles and the role of bilayer curvature. *Biochemistry.* 20:3126–3133.
73. Duzgunes, N., J. Wilschut, R. Fraley, and D. Papahadjopoulos. 1981. Studies on the mechanism of membrane fusion. Role of head-group composition in Ca^{+2} and Mg^{+2}-induced fusion of mixed phospholipid vesicles. *Biochim. Biophys. Acta.* 642:182–195.
74. Hoekstra, D., and O. C. Martin. 1982. Transbilayer redistribution of phosphatidylethanolamine during fusion of phospholipid vesicles. Dependence on fusion rate, lipid phase separation, and formation of nonbilayer structures. *Biochemistry.* 21:6097–6103.
75. Noordam, P. C., C. J. A. Van Echteld, B. DeKruijff, and J. DeGier. 1981. Rapid transbilayer movement of phosphatidylcholine in unsaturated phosphotidylethanolamine-containing model membranes. *Biochim. Biophys. Acta.* 646:483–487.
76. Hoekstra, D. 1982. Role of lipid phase separation and membrane hydration in phospholipid vesicle fusion. *Biochemistry.* 21:2833–2840.
77. Tilcock, C. P. S., and P. R. Cullis. 1981. The polymorphic phase behavior of mixed phosphatidylserine-phosphatidylethanolamine model systems as detected by ^{31}P-NMR. Effects of divalent cations and pH. *Biochim. Biophys. Acta. 641:189–201.*
78. Wilschut, J., and D. Papahadjopoulos. 1979. Ca^{+2}-induced fusion of phospholipid vesicles monitored by mixing of aqueous contents. *Nature (Lond.).* 281:690–692.
79. Wilschut, J., N. Duzguines, R. Fraley, and D. Papahadjopoulos. 1980. Studies on the mechanism of membrane fusion: kinetics of Ca^{+2}-induced fusion of phosphatidylserine vesicles followed by a new assay for mixing of aqueous vesicle contents. *Biochemistry.* 19:6011–6021.
80. Sundler, R., N. Duzgunes, and D. Papahadjopoulos. 1981. Control of membrane fusion by phospholipid headgroups. II. The role of phosphatidylethanolamine in mixtures with phosphatidate and phosphatidylinositol. *Biochim. Biophys. Acta.* 649:751–758.
81. Harlos, K., and H. Eibl. 1981. Hexagonal phases in phospholipids with saturated chains: phosphatidylethanolamines and phosphatidic acids. Biochemistry. 20:2888–2892.
82. Nayar, R., S. L. Schmid, M. J. Hope, and P. R. Cullis. 1982. Structural preferences of phosphatidylinositolphosphatidylethanolamine model membranes. Influence of Ca^{+2} and Mg^{+2}. *Biochim. Biophys. Acta.* 688:169–176.